



University Mohamed Khider of Biskra
Faculty of Exact Sciences and Nature and Life
Department of Matter Sciences

Final Dissertation in Master

Matter Sciences
Physics
Energy Physics and Renewable Energies

Réf. :

Presented by :

ARBIA HIZIA

Le : jeudi 27 juin 2019

The effect of permittivity on CIGS solar cells

Jury :

Dr. Boudib Ouahiba	M.C."A"	<i>University Med Khider of Biskra</i>	President
Dr. Sengouga Nouredine	Professor	<i>University Med Khider of Biskra</i>	Reporter
Dr. Soltani Mohamed Toufik	Professor	<i>University Med Khider of Biskra</i>	Examiner

Academic Year: 2018-2019



AKnowledgments

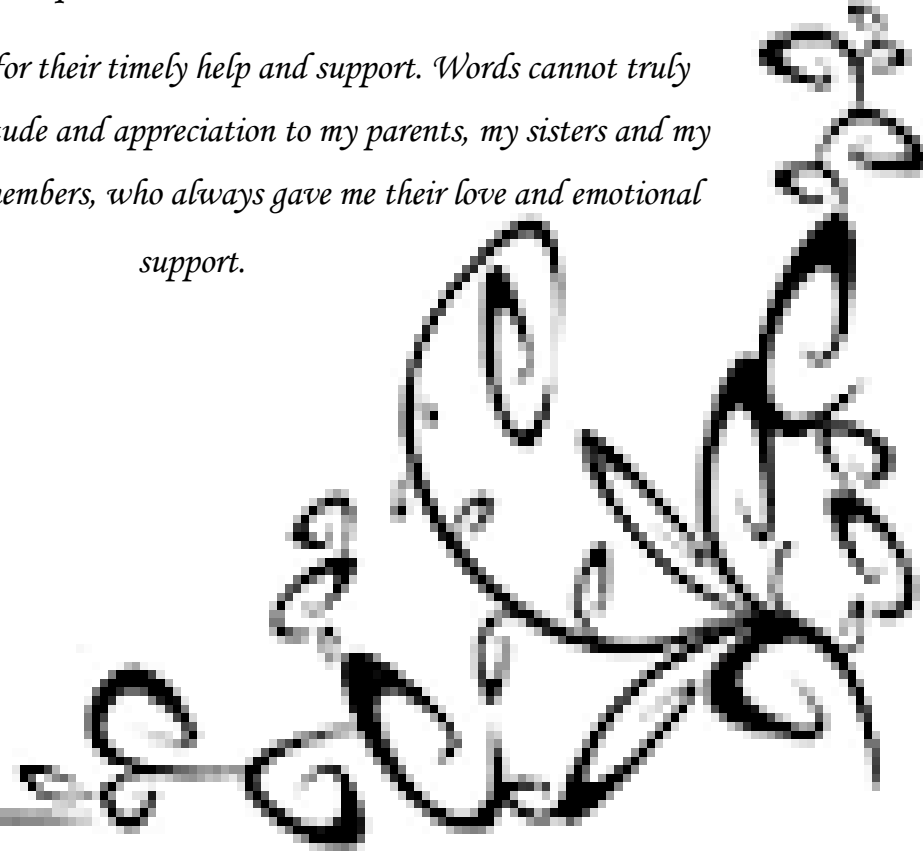
First and foremost, I would like to take this opportunity to thank my advisor, Professor Sengouga Noureddine for his help and support throughout this work,

I enjoyed working under his supervision and appreciate his constant guidance and encouragement. It really was a great experience and an overall growth of personality.

Besides my supervisor, I am very grateful to the members of the jury: Professor. Soltani Mohamed Toufik, and Doctor .Boudib Ouahiba for accepting to judge this thesis.

I would like to acknowledge the help of Abdellaoui Maroua who accept my questions in all times.

I thank all my friends for their timely help and support. Words cannot truly express my deepest gratitude and appreciation to my parents, my sisters and my brother and all family members, who always gave me their love and emotional support.



LIST OF ABBREVIATIONS

I_{sc} :	The short circuit current (mA/cm ²).
V_{oc} :	The open circuit voltage (Volt).
FF:	The fill factor (%).
η :	The conversion efficiency (%).
I_s :	Saturation current (mA/cm ²).
I_{ph} :	Photo-generated current (mA/cm ²).
a-Si:	Amorphous silicon.
CdTe:	Cadmium telluride.
CIGS:	Copper indium gallium diselenide.
AM1.5:	The air mass.
E_g :	Band gap (eV).
χ :	Electron affinity (eV).
ϵ :	Dielectric permittivity (relative).
N_c, N_v :	The effective density of states for the conduction band and valence band respectively (atoms/ cm^3).
v_{thn}, v_{thp} :	Electron and hole thermal velocity respectively (cm/s).
μ_n, μ_p :	Electrons and holes mobilities respectively (cm ² /Vs).
N_A, N_D :	Concentration of acceptor and donor atoms respectively (cm^{-3}).
N_T :	Concentration of traps (defects) (cm^{-3}).

LIST OF TABLES

<i>Table II.1: Parameters of the chalcopyrite ternaries derived from CuInSe₂ are grouped together</i>	
<i>[27].....</i>	<i>18</i>
<i>Table II.2: Conduction type in CIS in function to the ratio $\left(\frac{\text{Cu}}{\text{In}}\right)$ and $\left(\frac{\text{Se}}{\text{Cu} + \text{In}}\right)$ [43].....</i>	<i>23</i>
<i>Table II.3: The efficiency of Cu(In, Ga)(S, Se)₂ absorbers based photovoltaic cells.....</i>	<i>29</i>
<i>Table IV.1: Properties of the three layers CIGS, CdS, i – ZnO.....</i>	<i>45</i>

LIST OF FIGURES

<i>Figure I.1: The photovoltaic effect.....</i>	<i>2</i>
<i>Figure I.2: The p-n junction [10].....</i>	<i>2</i>
<i>Figure I.3: Solar cell work principle.....</i>	<i>3</i>
<i>Figure I.4: Solar cell J-V characteristic.....</i>	<i>4</i>
<i>Figure I.5: Equivalent electrical circuit for an ideal solar cell [10].....</i>	<i>5</i>
<i>Figure I.6: The fill factor.....</i>	<i>6</i>
<i>Figure I.7: Mono-crystalline solar cell.....</i>	<i>9</i>
<i>Figure I.8 : Polycrystalline Solar cell.....</i>	<i>9</i>
<i>Figure I.9 : a-Si Solar cell.....</i>	<i>11</i>
<i>Figure I.10 : CdTe Solar cell.....</i>	<i>11</i>
<i>Figure I.11 : CIGS Solar cell.....</i>	<i>12</i>
<i>Figure I.12 : Polymer Solar cell.</i>	<i>13</i>
<i>Figure I.13 : Dye sensitized Solar cell.</i>	<i>14</i>
<i>Figure I.14 : Perovskite Solar cell.</i>	<i>15</i>
<i>Figure II.1: Unit cells of chalcogenide compounds. (a) Sphalerite or zinc blende structure of ZnSe (two unit cells); (b) chalcopyrite structure of CuInSe₂. The metal sites in the two unit cells of the sphalerite structure of ZnSe are alternately occupied by Cu and In in the chalcopyrite structure [3].....</i>	<i>18</i>
<i>Figure II.2: Comparison of the elementary meshes of the crystal structures of Si, CdTe and CIGS. Chalcopyrite structure after [26].</i>	<i>18</i>
<i>Figure II.3: Evolution of a and c mesh parameters values, and the ratio c/a as a function of the ratio Ga/(In + Ga) for the Cu(In_(1-x)Ga_x)Se₂ solid solution [27].....</i>	<i>20</i>
<i>Figure II.4: a) Ternary diagram of the Cu-In-Se system at room temperature .b) Pseudo-binary diagram of the intermediate compounds Cu₂Se and In₂Se [26].....</i>	<i>20</i>

<i>Figure II.5: E_g band-gap energies vs. a lattice constant of the Cu(In, Ga, Al)(S, Se)₂ alloy system [3].</i>	22
<i>Figure II.6: Absorption's coefficient of material (CuInSe, CdTe, GaAs, aSi: H mono Si and CdS) for the manufacture of cells solar in thin films [44].</i>	24
<i>Figure II.7: Standard structure of CIGS based solar cells.</i>	25
<i>Figure II.8: Bands diagram of a CIGS/CdS/ZnO cell.</i>	27
<i>Figure III.1: The SCAPS start-up panel, the Action panel or main panel.</i>	33
<i>Figure III.2: Define the problem.</i>	34
<i>Figure III.3: The working point.</i>	35
<i>Figure III.4: Calculate single shot.</i>	36
<i>Figure III.5: The energy band panel.</i>	36
<i>Figure III.6: I-V curve display panel in the dark and in light.</i>	37
<i>Figure III.7: Defining a solar cell structure.</i>	38
<i>Figure III.8: Contact properties panel.</i>	39
<i>Figure III.9: Properties of the added layer.</i>	40
<i>Figure III.10: Properties of defined doping.</i>	41
<i>Figure III.11: The absorption model.</i>	41
<i>Figure III.12: Definition of recombination types.</i>	41
<i>Figure IV.1: Simplified diagram of a solar cell in CIGS thin layer.</i>	44
<i>Figure IV.2: (a) The J-V characteristic, (b) the quantum efficiency for CdS layer.</i>	46
<i>Figure IV.3: The effect of the relative permittivity of CdS layer in: (a) open circuit voltage, (b) short circuit current density, (c) the fill factor, (d) the efficiency.</i>	47
<i>Figure IV.4: (a) The J-V characteristic for ZnO window layer where $\epsilon(\text{CdS}) = 10$ and $\epsilon(\text{CIGS}) = 13.6$, (b) the quantum efficiency.</i>	48
<i>Figure IV.5: The effect of the relative permittivity of ZnO window layer in: (a) open circuit voltage, (b) short circuit current density, (c) the fill factor, (d) the efficiency.</i>	49

*Figure IV.6: (a) The J-V characteristic for **ZnO** window layer where $\epsilon_{(cds)} = 15$ and $\epsilon_{(cigs)}$ layer is constant and equal to 13.6, (b) quantum efficiency.....50*

*Figure IV.7: The effect of the relative permittivity of **ZnO** window layer in: (a) open circuit voltage, (b) short circuit current density, (c) the fill factor, (d) the efficiency.....51*

Figure IV.8: (a) The J-V characteristic for CIGS absorber layer where $\epsilon_{(cds)} \epsilon_{(zno)}$ equal to 15, (b) quantum efficiency.....52

Figure IV.9: The effect of the relative permittivity of CIGS absorber layer in: (a) open circuit voltage, (b) short circuit current density, (c) the fill factor, (d) the efficiency.....53

TABLE OF CONTENTS

KNOWLEDGMENT.....	II
LIST OF ABBREVIATIONS.....	III
LIST OF TABLES.....	IV
LIST OF FIGURES.....	X
GENERAL INTRODUCTION	XI
CHAPTER I: Generalities about solar cells	0
I.1 Introduction	1
I.2 The photovoltaic effect (PV).....	2
I.3 The p-n junction	2
I.4 The solar cell	3
I.4.1 Definition.....	3
I.4.2 Solar cell work principle.....	3
I.4.3 Current -voltage characteristics of a solar cell.....	4
I.4.4 Equivalent electrical circuit of a solar cell.....	5
I.4.5 Figures of merit of a solar cell.....	5
I.4.5.1 Short circuit current (I_{sc}).....	5
I.4.5.2 The open-circuit voltage (V_{oc}).....	5
I.4.5.3 The maximum power (P_m).....	6
I.4.5.4 Fill factor (FF).....	6
I.4.5.5 Efficiency (η).....	7
I.4.5.6 The Quantum Efficiency.....	7
I.4.5.7 The spectral response ($SR(\lambda)$).....	7
I.4.6 The three generations of solar cells.....	8
I.4.6.1 First Generation Solar Cell-Wafer Based.....	8
I.4.6.1.a Single/Mono-Crystalline Silicon solar cell.....	8
I.4.6.1.b Polycrystalline Silicon Solar Cell (Poly Si or Mc-Si).....	9
I.4.6.2 Second generation solar cell –thin film solar cells.....	10

I.4.6.2.a	Amorphous Silicon Thin Film (a-Si) Solar Cell.....	10
I.4.6.2.b	Cadmium Telluride CdTe Thin Film Solar Cell.....	11
I.4.6.2.c	CIS/CIGS/CIGSS thin film solar cell.....	12
I.4.6.3	Third Generation Solar Cells.....	12
I.4.6.3.a	Nano Cristal Based Solar Cells.....	12
I.4.6.3.b	Polymer Solar Cell.....	13
I.4.6.3.c	Dye-Sensitized Solar Cell (DSSC).....	13
I.4.6.3.d	Organic solar cell.....	14
I.4.6.3.e	Perovskite Solar Cell.....	15
CHAPTER II: CIGS based solar cells.....		16
II.1	Introduction.....	17
II.2	CuInSe ₂ structure(CIS)	17
II.3	Pseudo-binary phase diagram of the Cu-In-Se system	20
II.4	Semiconductor Properties and Gap Adjustment	21
II.5	Electrical properties.....	22
II.6	Optical properties of CuInSe ₂	23
II.7	The structure of CIGS based solar cells.....	25
II.8	The layers constitute the CIGS based solar cell	25
II.8.1	The substrate.....	25
II.8.2	The Back Contact.....	25
II.8.3	The CIGS absorber material.....	26
II.8.4	The buffer layer.....	26
II.8.5	The window layer.....	27
II.8.6	The front contact.....	27
II.9	The performance of a CuInSe ₂ based solar cell.....	28
II.10	Features and disadvantages.....	29
II.10.1	Features.....	29
II.10.2	Disadvantages.....	30

CHAPTER III: SCAPS software.....	31
III.1 Introduction	32
III.2 The basics	33
III.2.1 Run SCAPS.....	34
III.2.2 Define the problem.....	34
III.2.3 Define the working point.....	34
III.2.4 Select the measurement(s) to simulate.....	35
III.2.5 Start the calculation(s).....	35
III.2.6 Display the simulated curves.....	36
III.2.7 The I-V curves.....	36
III.3 Solar cell definition	37
III.3.1 Edition a Solar cell structure.....	38
III.3.2 Contacts.....	38
III.3.3 Definitions of layers.....	39
CHAPTER IV: Results and discussion.....	43
IV.1 Introduction	44
IV.2 The structure of the studied solar cell	44
IV.3 The studied device parameter	45
IV.4 Result and discussion	45
IV.4.1 The effect of the relative permittivity on CIGS figures of merit.....	45
IV.4.1.1 The influence of the relative permittivity of CdS layer.....	45
IV.4.1.2 The influence of the relative permittivity of i – ZnO layer.....	47
IV.4.1.3 The influence of the relative permittivity of CIGS absorber layer.....	51
GENERAL CONCLUSION.....	54
REFERENCES.....	55
ABSTRACT.....	59



General

introduction

General introduction

The energy is listed as the first priority of the humanity for the next years. It is widely used in industry, transport, communication, agriculture and in daily life. It comes under multiple forms divided in two main categories. The first is the category of energy called non renewable, extract of coal, gas, oil and of uranium. The second is that of energy called renewable as the wind turbine, the biomass, geothermal, hydroelectric, solar thermal and photovoltaic or what we called solar energy.

Solar energy is the most promising source of energy of modern area. It has a biggest advantage over the conventional power generation systems that the sunlight can be directly converted into solar energy with the help of solar cells. This type of electrical energy production methods is cost effective, generates no toxic materials, and follows green approach. The modern photovoltaic technology follow the principle that, each cell consists of two different layers of semiconducting materials i.e. p type material and n type material. When photon of appropriate energy strikes this combination of materials an electron by acquiring energy from photon moves from one layer to another and consequently generates electricity. Modern technologies are using this phenomenon for production of solar cells but less efficiency and high cost are major setback for them.

In previous many year, silicon wafer has been the prominent material used for fabrication of solar cells but due to high cost and low efficiency, it has gradually lost the interest of researchers. Nowadays, other materials appear to be competitive with silicon, among them the chalcopyrite structured semiconductors of the CIS-based family $(\text{Cu}(\text{In}, \text{Ga}, \text{Al})(\text{Se}, \text{S})_2$ [1], where conversion efficiencies of up to 20.3% have been demonstrated on rigid glass substrates [2]. Indeed, these compounds have bandwidths between 1 eV (CuInSe_2) and 3 eV (CuAlS_2) which allows them to absorb most of the solar radiation, and these materials are today the ones that make it possible to achieve the highest photovoltaic conversion efficiencies from thin film devices [3, 4]. In particular $\text{Cu}(\text{In}, \text{Ga})\text{Se}_2$, which is considered to be the most efficient among all CIS-based solar cells [4]. The interest in CIGS thin film solar cells has increased significantly due to its promising characteristics for high performance and low cost [5].

The objective of the present thesis is to study the effect of the permittivity on CIGS based solar cells figures of merit by a numerical simulation with SCAPS software [6].

This thesis is divided into four chapter:

- ❖ The first chapter is generalities about solar cells (definition, working principle, the I-V characteristics, electrical circuit equivalence, the different figures of merit and generations).
- ❖ The second chapter is about general properties of CIGS based solar cells.
- ❖ The third chapter is about SCAPS software.
- ❖ The fourth includes simulation results and discussion.



CHAPTER I:

Generalities about solar cells

I.1 Introduction

Solar energy is the most promising source of energy of modern area. It has a biggest advantage over the conventional power generation systems that the sunlight can be directly converted into solar energy with the help of solar cells. This type of electrical energy production methods is cost effective, generates no toxic materials and follows green approach. The sun light can easily compensate the energy drawn from the non-renewable sources of energy such as fossil fuels and petroleum deposits inside the earth. The fabrication of solar cells has passed through a large number of improvement steps from one generation to another. Silicon based solar cells were the first-generation solar cells grown on Si wafers, mainly single crystals. Further development to thin films, dye sensitized solar cells and organic solar cells enhanced the cell efficiency. The development is hindered by the cost and efficiency [7, 8].

In this chapter, we will talk about the photovoltaic effect, the p-n junction and we cite some concepts about solar cells, including their (definition, working principle, the current –voltage characteristics, electrical circuit equivalence, and the different figures of merit) and we will conclude with a short description of the various existing generations.

I.2 The photovoltaic effect (PV)

A French physicist, Edmund Becquerel, first observed the physical phenomenon responsible for converting light to electricity -the photovoltaic effect-in 1839 [7]. Becquerel noted a voltage appeared when one of two identical electrodes, in a weak conducting solution, was illuminated. It is the basis of the conversion of light to electricity in photovoltaic or solar cells. Simply described, the PV effect is as follows: light, which is pure energy, enters a PV cell and imparts enough energy to some electrons (negatively charged atomic particles) to become free. A built-in-potential barrier in the cell acts on these electrons to produce a voltage (called photo-voltage), which can be used to drive a current through a circuit [7]. The **Figure I.1** represent the photovoltaic effect.

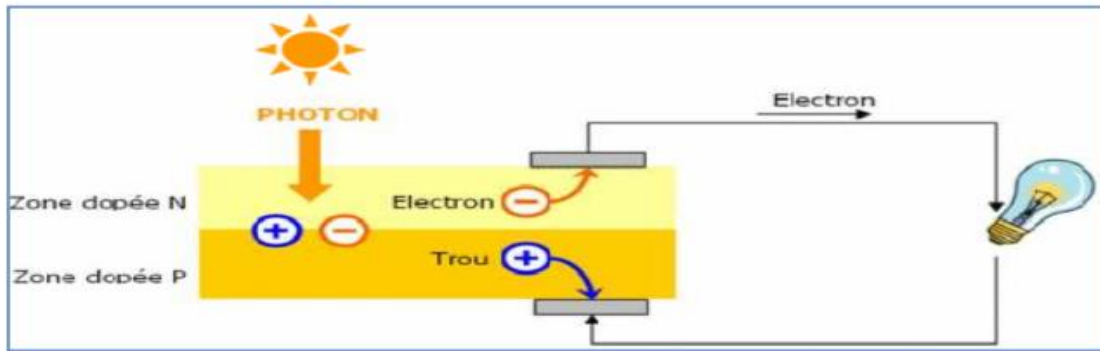


Figure I.1: The photovoltaic effect.

I.3 The p-n junction

When we assemble (using special techniques) two semiconductor materials, one of type P and the other of type N, like in “**Figure I.2**“, we obtain what is called a PN junction. When the two types of semiconductors come into contact, the electrons, which are the majority in the N side, will diffuse, under the effect of the concentration gradient, towards the P side and similarly, the holes in the P side will diffuse towards the N side [9].

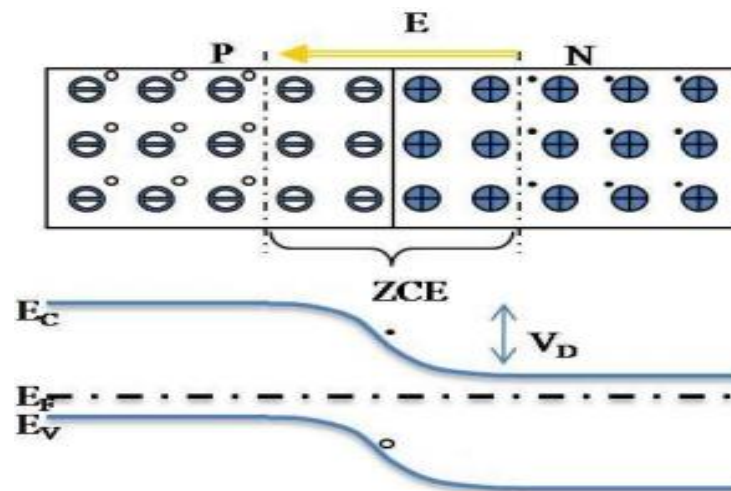


Figure I.2: The p-n junction [10].

There are two type of p-n junctions:

- ❖ Steep junction (step junction): the transition from the region "P" to the region "N" takes place on an infinitely fine thickness.
- ❖ Gradual junction (linearly graded junction): the transition from the region "P" to the region "N" takes place according to a linear law [11].

I.4 The solar cell

I.4.1 Definition

Solar cell is a device that converts energy from the sun directly into electrical energy. It provides the longest-lasting source of energy for satellites and space vehicles. It has also been successfully implemented in several small-scale terrestrial applications. Its importance has not stopped growing, especially since the world has come to realize that, it must develop other energy resources other than conventional resources. The best candidate for this function is the sun [12, 13].

I.4.2 Solar cell work principle

The heart of the solar energy generation system is the solar cell. It consists of three major elements namely:

- The semiconductor material which absorbs photons (whose energy is greater than the gap) and generates an electron-hole pair.
- The junction formed within the semiconductor, which separates the photo-generated carriers (electrons and holes) electrons to the negative terminal and holes to the positive terminal.
- The contacts on the front and back of the cell that allow the current to flow to the external circuit [14].

Figure I.3 show the solar cell work principle.

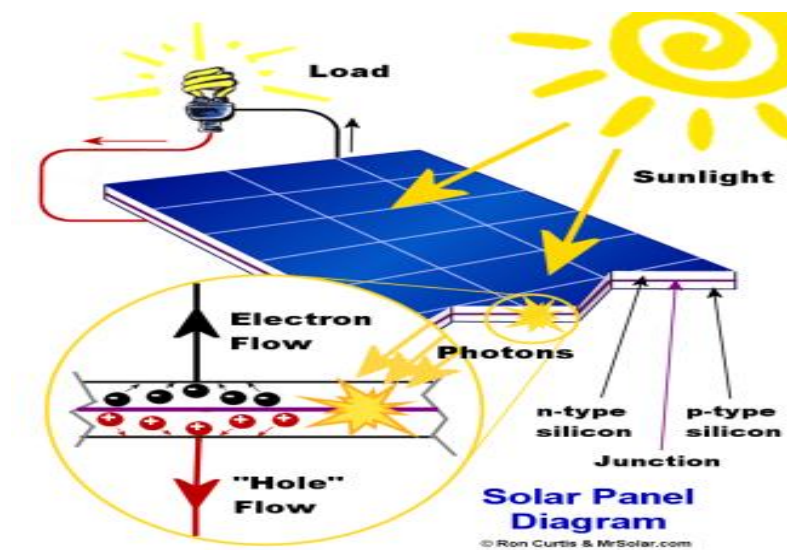


Figure I.3: Solar cell work principle.

I.4.3 Current -voltage characteristics of a solar cell

The characteristic curve of a PV cell represents the variation of the current that it produces as a function of the voltage at the terminals of the PV cell. In fact, the operation of the photovoltaic cells depends on the sunlight and temperature conditions on the surface of the cell. Thus, each current-voltage curve corresponds to specific operating conditions at fixed temperatures for the two regimes under darkness and under illumination [9, 15].

The following relation gives the current through a p-n junction diode in dark:

$$I = I_{sat} \left(e^{\frac{qV}{K_B T}} - 1 \right) \quad \text{I.1}$$

Where I_{sat} is the saturation current in reverse bias under zero illumination, q is the electronic charge, V is the applied voltage, K_B is Boltzmann's constant, T is the temperature of the cell.

An ideal diode characteristic for an illuminated cell is shown in **Figure I.4**. In the dark the J–V plot would go through the origin and as the light intensity increases, the short-circuit current becomes increasingly negative, indicating the presence of a photo-generated current [9, 15].

The equation for the I-V characteristic of this ideal device is:

$$I = I_{sat} \left(e^{\frac{qV}{K_B T}} - 1 \right) - I_{ph} \quad \text{I.2}$$

I_{ph} is the photogenerated current. A characteristic current voltage of a cell at the rising pace:

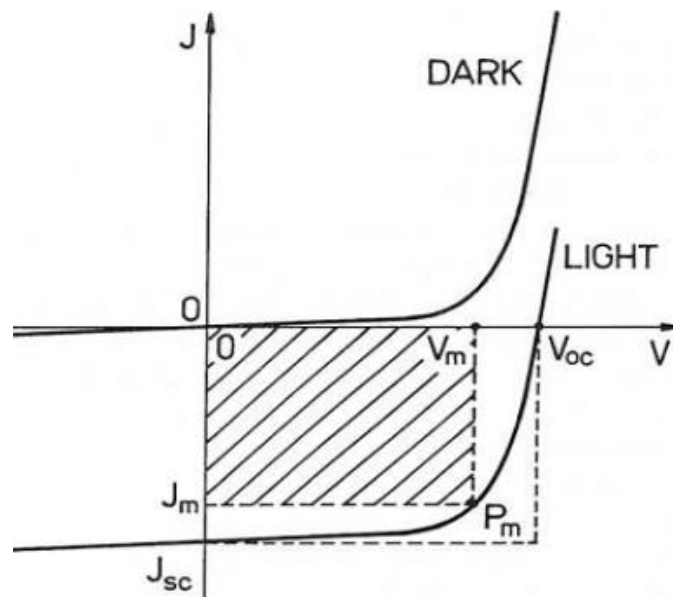


Figure I.4: Solar cell J-V characteristic.

This characteristic is shifted downwards by a current I_{sc} (short circuit current). Similarly, it cuts the abscise axis in V_{oc} (maximum open circuit voltage).

I.4.4 Equivalent electrical circuit of a solar cell

The operation of a solar cell can be modeled by considering the electrical equivalent diagram below “**Figure I.5**”. We can consider the case of an ideal photovoltaic cell comprising current generated by the photons and the diode, which models the p-n junction, a current source and a diode in parallel. The current source models to consider the case of a real photovoltaic cell. The equivalent circuit must integrate [15]:

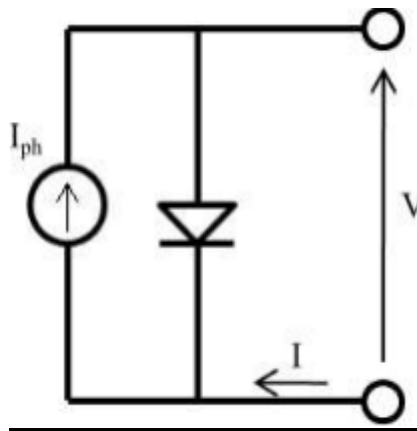


Figure I.5: Equivalent electrical circuit for an ideal solar cell [10].

I.4.5 Figures of merit of a solar cell

I.4.5.1 Short circuit current (I_{sc})

The short-circuit current is the current of a solar cell under standard illumination conditions when the load has zero resistance. In this case, the voltage is zero. It means:

For an ideal solar cell, the short circuit current is equal to the photovoltaic current I_{ph} .

$$I_{sc}(V = 0) = I_{ph} \quad \mathbf{I.3}$$

I.4.5.2 The open-circuit voltage (V_{oc})

The open circuit voltage V_{oc} is the maximum voltage that can generate the cell. It is the voltage between the terminals of a solar cell under standard illumination conditions when the load has

infinite resistance that is open, in this situation, the current flowing through the cell is zero ($I = 0$). It is given by the relation:

$$V_{oc} = \frac{k_B T}{q} \ln\left(\frac{I_{sc}}{I_s} + 1\right) \quad \text{I.4}$$

I.4.5.3 The maximum power (P_m)

The operating point is imposed by the load resistance and not by the cell itself. A judicious choice of the load resistance will thus make it possible to obtain the maximum power, either

$$P_{max} = I_m \times V_m \quad \text{I.5}$$

I.4.5.4 Fill factor (FF)

The fill factor or FF gives us an overview of the cell quality. It is the ratio between the maximum power outputs $V_m \cdot I_m$ (The surface of the smallest rectangle) and the ideal power $V_{oc} \cdot I_{sc}$ (The surface of the largest rectangle), where V_m and I_m are the voltage and current value corresponding to the operating point P_m for which the power is maximum. The following relation gives the FF:

$$FF = \frac{P_{max}}{V_{oc} \times I_{sc}} = \frac{V_m \times I_m}{V_{oc} \times I_{sc}} \quad \text{I.6}$$

The fill factor is shown in “Figure I.6 “below:

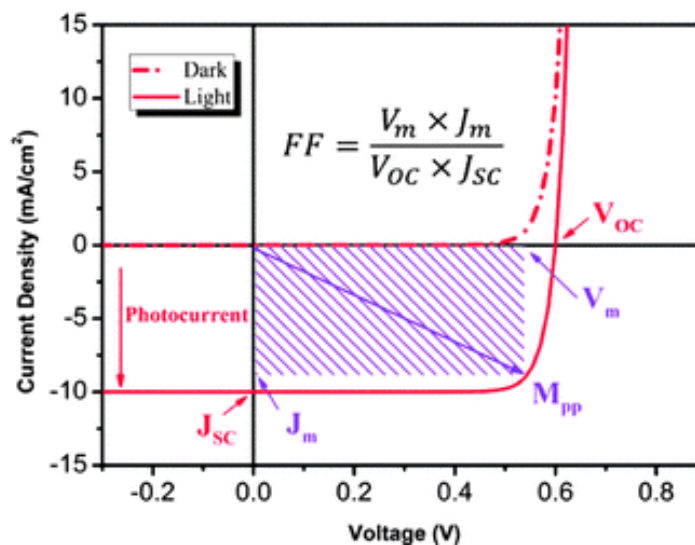


Figure I.6: The fill factor.

I.4.5.5 Efficiency (η)

From these parameters (V_{oc} , I_{sc} and FF), it is possible to determine the efficiency of the cell, which is the most important parameter since it allows the evaluation of the performance of the PV cell. It is defined as the percentage associated with the ratio between the power generated by the cell (P_{cell}) and the incident power (P_{in}) of the light radiation illuminating the cell. It is calculated according to the following formula [16]:

$$(\eta) = \frac{P_{max}}{P_{in}} \times 100\% = \frac{V_m \times I_m}{P_{in}} \times 100\% = \frac{FF \times V_{oc} \times I_{sc}}{P_{in}} \times 100\% \quad \mathbf{I.7}$$

Power conversion efficiency is important since it determines how effectively the space occupied by a solar cell is being used and how much area must be covered with solar cells to produce a given amount of power. Since larger areas require more resources to cover with solar cells, higher (η) is often desirable. We can improve it by increasing the short current circuit, the open circuit voltage and the fill factor.

I.4.5.6 The Quantum Efficiency

The quantum efficiency of a solar cell is defined as the ratio of the number of electrons in the external circuit produced by the number of an incident photon of a given wavelength. Thus, one can define external and internal quantum efficiency denoted by $EQE(\lambda)$ and $IQE(\lambda)$ respectively. They differ in the treatment of photons reflected from the cell; all photons hitting on the cell surface are taken into account in the value of the $EQE(\lambda)$ but only photons that are not reflected are considered in the value of $IQE(\lambda)$ [17]. The following relation gives the quantum efficiency:

$$QE(\lambda) = \frac{1}{q} \times \frac{hc}{\lambda} \times \frac{I_{sc}(\lambda)}{P_{in}(\lambda)} \quad \mathbf{I.8}$$

I.4.5.7 The spectral response (SR (λ))

The spectral response (SR (λ)), with the unit (A/W) is defined as the ratio of the photocurrent generated by a solar cell under monochromatic illumination on the incident power $P_{in}(\lambda)$ for each wavelength, the spectral response can be written in terms of the quantum efficiency as [17]:

$$SR(\lambda) = \frac{q\lambda}{hc} \times QE(\lambda) \quad \mathbf{I.9}$$

Where λ is in micrometer. Spectral response can be either internal or external, depending on which value is used for the quantum efficiency.

I.4.6 The three generations of solar cells

The photovoltaic solar cells are categorized into various classes as discussed in the following sections:

I.4.6.1 First Generation solar cell-wafer based

This type of cell is based on a single p-n junction and generally used silicon in crystalline form as a semiconductor material. This was the beginning of the "first generation" of solar cells made from a solid silicon substrate derived from ingot printing and platelet cutting. This production method based on silicon wafers is very energy intensive and therefore very expensive. It also requires a silicon of high purity [12].

As it is already mentioned, the first-generation solar cells are produced on silicon wafers it is the oldest and the most popular technology due to high power efficiencies. The silicon wafer-based technology is further categorized into two subgroups named as:

- ✚ Single/ Mono-crystalline silicon solar cell.
- ✚ Poly/Multi-crystalline silicon solar cell [8].

I.4.6.1.1 Single/Mono-crystalline silicon solar cell

Are produced by growing high purity, single crystal Si rods and slicing them into thin wafers. Single crystal wafer cells are expensive. They are cut from cylindrical ingots and do not completely cover a square solar module. To save material and space, the solar cells are cut to an octagonal piece. Mono crystalline solar cell, as the name indicates, is manufactured from single crystals of silicon by a process called Czochralski process. During the manufacturing process, Si crystals are sliced from the big sized ingots. There is always some wasted space because of the cut corners. These large single crystal productions require precise processing, as the process of "recrystallizing" the cell is more expensive and multi process. The efficiency of mono-crystalline single-crystalline silicon solar cells lies between 17% - 18 %. Solar cells are usually perfect squares; there is no wasted space [8, 14, 16]. The "Figure I.7" show the mono-crystalline solar cell.



Figure I.7: Mono-crystalline solar cell

I.4.6.1.2 Polycrystalline silicon solar cell (Poly Si or Mc-Si)

Polycrystalline PV modules are generally composed of a number of different crystals, coupled one to another in a single cell. The polycrystalline solar cells “**Figure I.8**” are cut from a rectangular ingot [8, 16]. The processing of polycrystalline Si solar cells is more economical, which are produced by cooling a graphite mold filled containing molten silicon. Polycrystalline Si solar cells are currently the most popular solar cells. They are believed to occupy most up to 48% of the solar cell production worldwide during 2008. During solidification of the molten silicon, various crystal structures are formed. Though they are slightly cheaper to fabricate compared to mono-crystalline silicon solar panels, yet are less efficient than ~12% - 14 % [8].

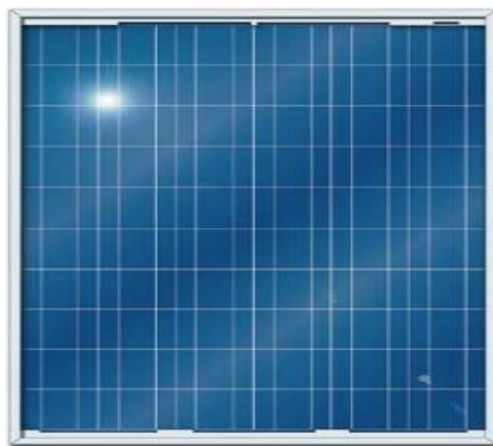


Figure I.8: Polycrystalline solar cell.

Crystalline silicon solar cells at the commercial level have achieved efficiencies of as much as 16%, whereas experimental developments have achieved efficiencies of more than 24% [18].

I.4.6.2 Second generation solar cell –thin film solar cells

Second-generation solar cells are also known as thin-film solar cells because when compared to crystalline silicon-based cells, they are made from layers only a few micrometers thick. After more than 20 years of R&D, thin-film solar cells are beginning to be deployed in significant quantities. Thin-film solar cells could potentially provide lower cost electricity than c-Si wafer-based solar cells [19].

Thin film solar cells are classified as;

- a-Si
- CdTe
- CIGS [8].

I.4.6.2.1 Amorphous silicon thin film (a-Si) solar cell

Amorphous silicon offers the potential for a cheap production technology for terrestrial photovoltaic solar cells. The most common method for producing a-Si: H for photovoltaic is by plasma-enhanced CVD from SiH₄ mixtures. The film is deposited onto a textured conducting oxide such as indium-tin oxide (ITO), which provides the electrical contact and increases the average light path in the absorber layer to increase absorption. The device structure is a p-i-n with absorption taking place in the middle (insulator) layer, which is only 0.5µm thick [20]. Amorphous Si (a-Si) PV modules are the primitive solar cells that are first to be manufactured industrially is can be manufactured at a low processing temperature, various low cost, polymer and other flexible substrate. These substrates require a smaller amount of energy for processing. Therefore, a-Si amorphous solar cell”**Figure I.9**” is comparatively cheaper and widely available. Currently, the efficiencies of commercial PV modules vary in the range of 4% - 8%. They can be easily operated at elevated temperatures, and are suitable for the changing climatic condition where sun shines for few hours [8].



Figure I.9 : a-Si solar cell.

I.4.6.2.2 Cadmium Telluride $CdTe$ thin film solar cell

Cadmium telluride ($CdTe$) photovoltaic, describes a photovoltaic (PV) technology that is based on the use of cadmium telluride, a thin semiconductor layer designed to absorb and convert sunlight into electricity. Cadmium telluride PV is the only thin film technology with lower costs than conventional solar cells made of crystalline silicon in multi-kilowatt systems [13]. It has a band gap of ~ 1.5 eV as well as high optical absorption coefficient and chemical stability. These properties make $CdTe$ most attractive material for designing of thin-film solar cells, another advantage is its compatibility with CdS , a wide-band-gap semiconductor for which it is easy to generate an n-type film. Because the absorption edge of CdS is 2.4 eV. It is transparent to the bulk of solar radiation. Its efficiency usually operates in the range 9%-11% [8]. **Figure I.10** describe the $CdTe$ solar cell:



Figure I.10 : $CdTe$ solar cell

I.4.6.2.3 CIS/CIGS/CIGSS thin film solar cell

CIGS is a quaternary compound semiconductor comprising of the four elements, namely: Copper, Indium, Gallium and Selenium. CIGS are also direct band gap type semiconductors. Compared to the C_dT_e thin film solar cell, CIGS hold a higher efficiency ~10% - 12%. Due to their significantly high efficiency and economy, CIGS based solar cell technology forms one of the most likely thin film technologies. The processing of CIGS are done by the following techniques: sputtering, co-evaporation, electrochemical coating technique, printing and electron beam deposition [8]. **Figure I.11** below represent CIGS solar cell.

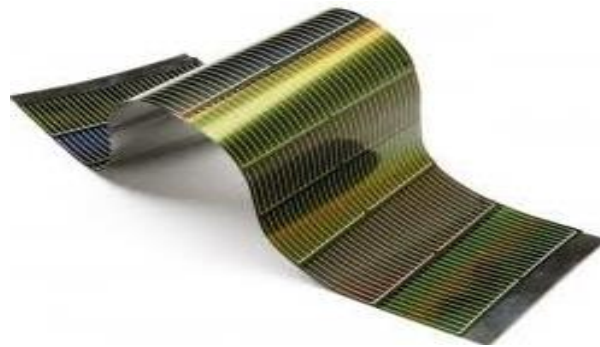


Figure I.11: CIGS solar cell.

I.4.6.3 Third Generation Solar Cells

Third generation cells are the new promising technologies but are not commercially investigated in detail:

- 1) Nano crystal based solar cells.
- 2) Polymer based solar cells.
- 3) Dye sensitized solar cells.
- 4) Organic photovoltaic.
- 5) Perovskite solar cell [8].

I.4.6.3.1 Nano Cristal Based Solar Cells

Nano crystal based solar cells are generally also known as Quantum dots (QD) solar cells. These solar cells are composed of a semiconductor, generally from transition metal groups, which are in the size of nano crystal range made of semiconducting materials. QD is just a name of the

crystal size ranging typically within a few nanometers in size, for example, materials like porous Si or porous TiO_2 , which are frequently used in QD. Nano crystal solar cells are solar cells based on a substrate with a coating of nano crystals. The nano crystals are typically based on silicon, C_dT_e or CIGS and the substrates are generally silicon or various organic conductor [13]. However, the efficiency is only around 2.5% compared to the theoretical efficiency of 44% [18].

I.4.6.3.2 Polymer solar cell

In this case the material used to absorb the solar light, is an organic material such as a conjugated polymer. A polymer solar cell “**Figure I.12**” is composed of a serially connected thin functional layers coated on a polymer foil or ribbon [8, 13].

The basic principle behind both the polymer solar cell and other forms of solar cells, however, is the same, namely the transformation of the energy in the form of electromagnetic radiation (light) into electrical energy (a current and a voltage), i.e. PV effect. Researchers achieved efficiency over 3 % [8, 13].



Figure I.12: Polymer solar cell

I.4.6.3.3 Dye-Sensitized Solar Cell (DSSC)

In early 1990, Michel Gratzel and coworkers from Swiss federal institute of technology designed mesoscopic cell or nanocrystalline dye sensitized solar cell using interpenetrating network of nanoscale titanium dioxide (TiO_2) covered with monolayer of sensitizing dye molecules with efficiency of 12%. The limitation of DSCs is poor optical absorption characteristics in near infrared region. Present sensitizers' possess' poor optical absorption

resulting in low conversion efficiency [1]. DSSC also sometimes referred to as dye sensitized cells (DSC), are a third generation photovoltaic (solar) cell that converts any visible light into electrical energy. DSSC were invented in 1991 by Professor Michael Grätzel and Dr Brian O'Regan at Ecole polytechnique Federal de Lausanne (EPFL), Switzerland and is often referred to as the cell, we call it G Cell [13]. This new class of advanced solar cell can be likened to artificial photosynthesis due to the way in which it mimics nature's absorption of light energy. Nevertheless, dye-sensitized solar cells have some disadvantages: first, the efficiency is about one-half of that of the crystalline silicon solar cells, second, the necessity of a liquid-phase electrolyte made the solar cell mechanically weak; third, the long-term stability of the organic materials needs to be improved [16]. this kind of solar cells is shown below in “**Figure I.13**”.

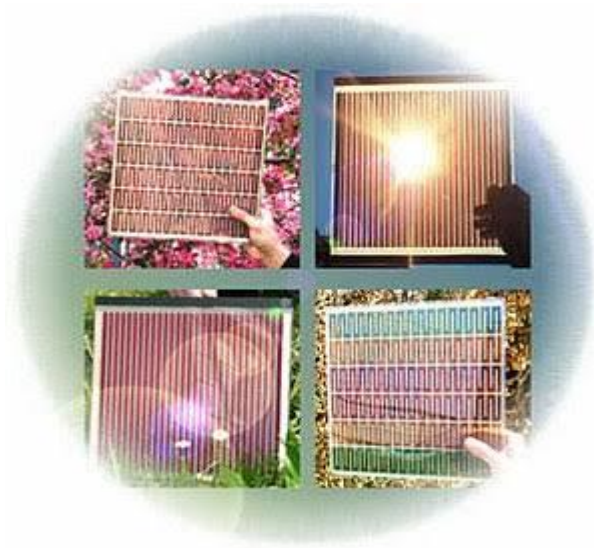


Figure I.13: Dye sensitized solar cell.

I.4.6.3.4 Organic solar cell

Organic solar cells are composed of organic or polymer materials (such as organic polymers or small organic molecules). They are inexpensive, but not very efficient. They are emerging as a niche technology, but their future development is not clear. Their success in recent years has been due to many significant improvements that have led to higher efficiencies. OPV module efficiencies are now in the range 8% to 10% for commercial systems. Organic cell production uses high-speed and low temperature roll-to-roll manufacturing processes and standard printing technologies [19].

I.4.6.3.5 Perovskite solar cell

The name 'perovskite solar cell' is derived from the ABX₃ crystal structure of the absorber materials, which is referred to as perovskite structure. The most commonly studied perovskite absorber is methyl-ammonium lead tri-halide (CH₃NH₃PbX₃), where X is a halogen ion such as I⁻, Br⁻ and Cl⁻, A and B are cations of different size., with an optical band gap between 2.3 eV and 1.6 eV, depending on halid content the perovskites based solar cells can have an efficiency up to 31%. It can be predicted that these perovskites may also play an important role in next generation electric automobiles batteries, according to an interesting investigation recently performed by Volkswagen however; current issues with perovskite solar cells” **Figure I.14**” are their stability and durability. The material degrades over time, and hence a drop in overall efficiency. Therefore, more research is needed to bring these cells into the market place [8, 13].

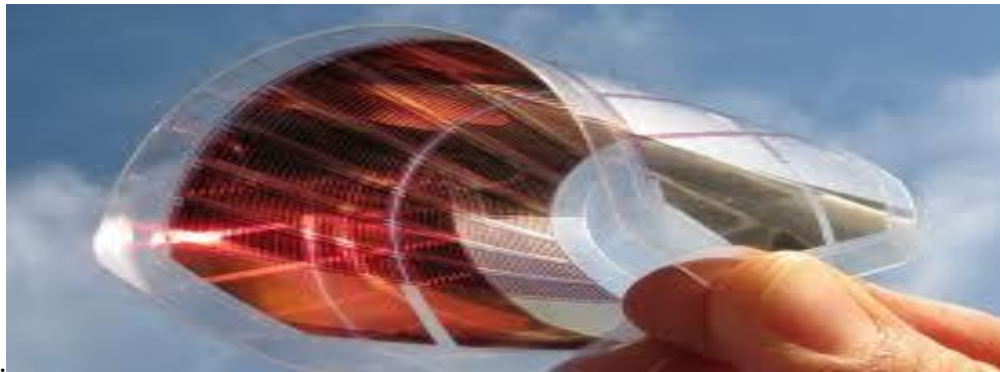
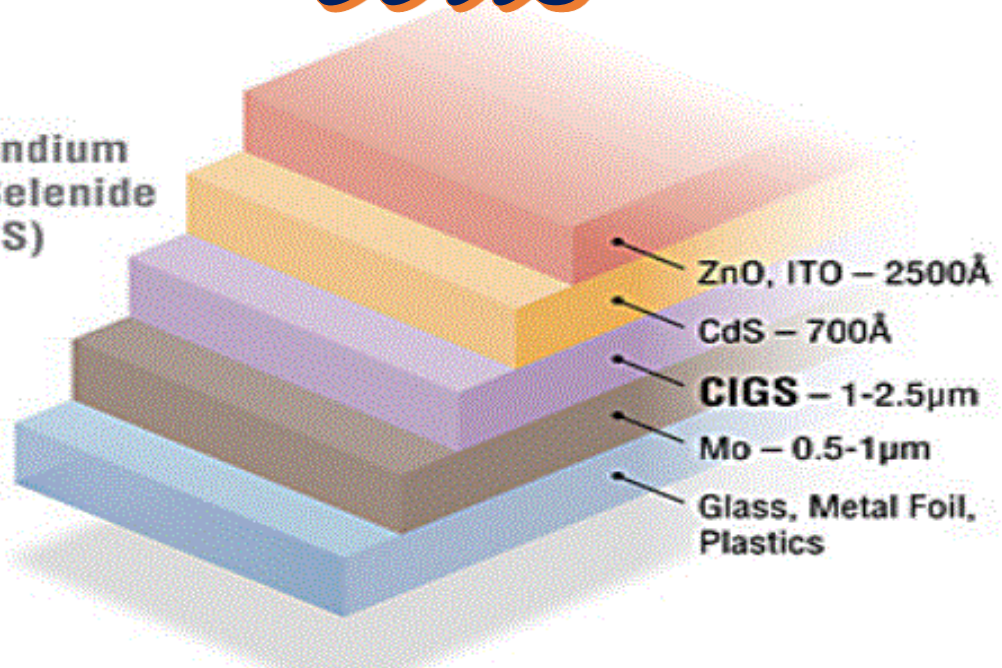


Figure I.14: Perovskite solar cell.

CHAPTER II:

CIGS based solar cells

Copper Indium
Gallium Selenide
(CIGS)



II.1 Introduction

Copper indium gallium (di) selenide Cu(In,Ga)Se_2 (CIGS) is an I-III-VI₂ semiconductor material composed of copper, indium, gallium, and selenium. The material is important for terrestrial applications of solar cells because of their high efficiency, long-term stable performance and potential for low-cost production. Thin film solar cells with polycrystalline Cu(In,Ga)Se_2 (CIGS) absorber layers provide a good alternative to wafer based crystalline silicon solar cells, which currently constitute the major share of photovoltaic installed and used worldwide. The CIGS based solar cells exhibit excellent outdoor stability, radiation hardness and highest efficiencies (19.2%) [21]. Cu(InGa)Se_2 -based solar cells have often been touted as being among the most promising of solar cell technologies for cost-effective power generation [22]. Solar cells based on chalcopyrite Cu(In,Ga)Se_2 (CIGS) absorbers are among the most promising thin-film photovoltaic technologies with Laboratory Scale Power Conversion Efficiencies (PCE) reaching 20.4% on a flexible polymer substrate and 22.6% on a soda lime glass (SLG) substrate [23]. Its development for solar cells began in the 1970s. Since then, device conversion efficiencies have exceeded 20% in the laboratory and reached 13% on an industrial scale. Although a CIGS cell consists of at least six different materials, it is mainly the understanding and improvement of the properties of the absorbing material that are at the heart of the progress made [24].

In this chapter, we will present, in the first part, general properties (structural, electrical and optical) of the material Cu(In,Ga)Se_2 (CIGS). The second part contain a description of CIGS based solar cells.

II.2 CuInSe_2 structure(CIS)

The material at the base of CIGS is CIS (CuInSe). It is a semiconductor with a tetragonal structure of chalcopyrite, corresponding to the superposition of two zinc-blende structures of II-VI materials such as ZnS (Figure II.1 (a)). Its unit cell is centered face of parameters: $\mathbf{a} = 5.785\text{\AA}$, $\mathbf{c} = 11.612\text{\AA}$ and $\mathbf{c}/\mathbf{a} = 2.006\text{\AA}$ [25]. The chalcopyrite structure of the tetragonal form is characterized by the alternation of the atoms of Cu and of In. Each atom of Se is tetrahedral bound to two atoms of Cu and of In while each atom of Cu or In is surrounded by four atoms of Se. The length of the bond Cu-Se is 2.43\AA and that of In is 2.57\AA , which gives a distortion tetragonal unit of 0.3% [25]. Figure II.1 (b) shows the structure of the molecule in CIS. In the case of CIGS, the sites of the group III atoms are therefore occupied by In or Ga atoms, in proportions depending on the composition of the alloy In other words, the CIGS is a

solid solution CuInSe_2 and CuGaSe_2 . Figure II.2 shows the differences in crystal structure between three semiconductors used in photovoltaic: Si, CdTe and CIGS.

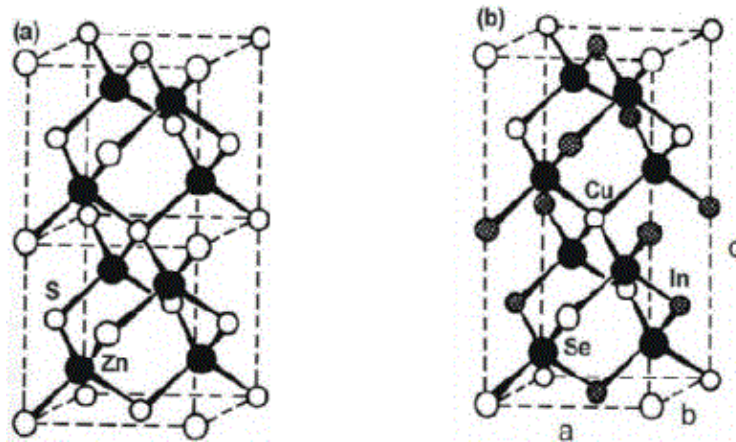


Figure II.1: Unit cells of chalcogenide compounds. (a) Sphalerite or zinc blende structure of ZnSe (two unit cells); (b) chalcopyrite structure of CuInSe_2 . The metal sites in the two unit cells of the sphalerite structure of ZnSe are alternately occupied by Cu and In in the chalcopyrite structure [3].

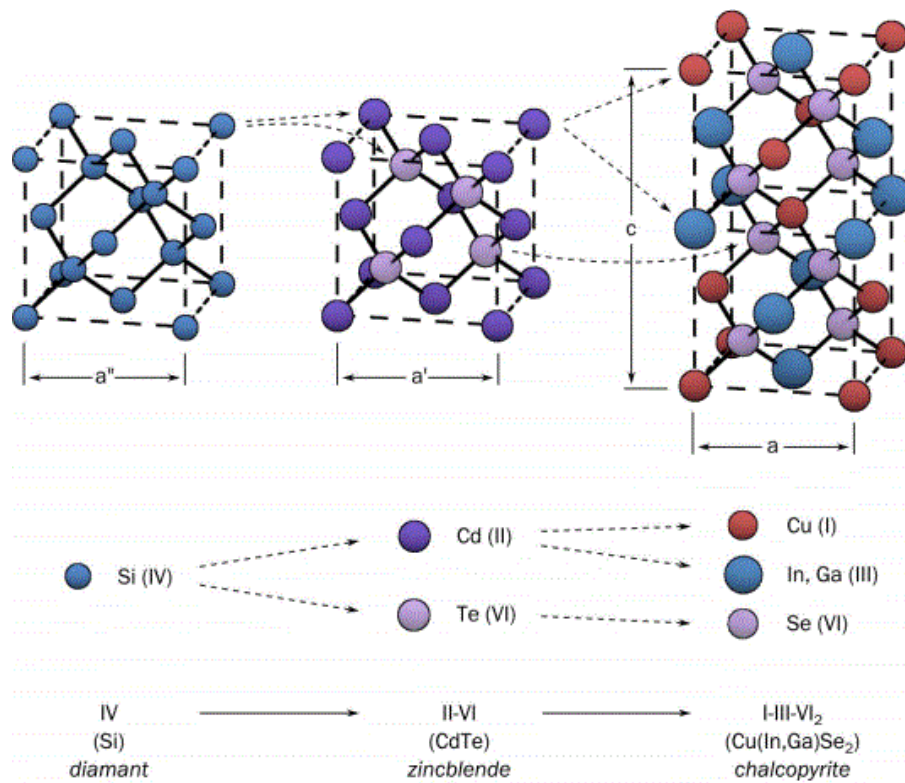


Figure II.2: Comparison of the elementary meshes of the crystal structures of Si, CdTe and CIGS. Chalcopyrite structure after [26]

Among the different compounds chalcopyrite ABX₂, we cite in particular the fourth ternary compounds: **CuInSe**, **CuGaSe₂**, **CuInS₂**, **CuGaS₂**[27]. all these compounds can sphalerite, chalcopyrite and **CuAu**. The change of atoms between each ternary modification of the length of links inter-elements, and done one modification of mesh. The values of reference compounds are listed in the following table:

Table II.1: Parameters of the chalcopyrite ternaries derived from CuInSe₂ are grouped together [27].

Ternary	a=b(Å)	c(Å)	c/a
CuInSe₂	5.7820	11.6190	2.0095
CuGaSe₂	5.6120	11.0320	1.9658
CuInS₂	5.5230	11.1200	2.0134
CuGaS₂	5.3600	10.4900	1.9571

The various alloys derived from CuInSe₂ are grouped under the term Cu(In_(1-x)Ga_x)Se₂. Alternatively, $x = \frac{\text{Ga}}{\text{Ga}+\text{In}}$ where is the Ga composition representing the level of gallium atoms, which replace the indium atoms in the structure.

The different quaternary solid solutions of: Cu(In_(1-x)Ga_x)Se₂ type, have been characterized by numerous authors. The evolution of the mesh parameters follows the Vegard law [28, 29], that is to say that the parameters evolve linearly between the values of the two associated ternaries. The evolution of quaternary Cu(In_(1-x)Ga_x)Se₂ lattice parameters is shown in **FigureII.3**.

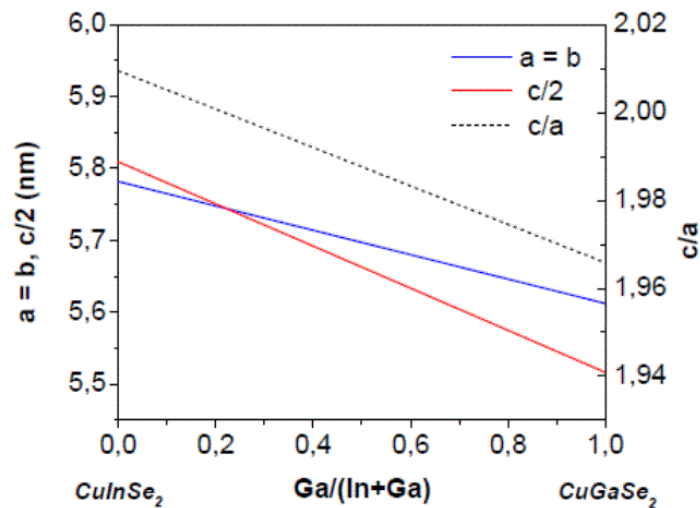


Figure II.3: Evolution of a and c mesh parameters values, and the ratio c/a as a function of the ratio $Ga/(In + Ga)$ for the $Cu(In_{(1-x)}Ga_x)Se_2$ solid solution [27].

II.3 Pseudo-binary phase diagram of the Cu-In-Se system

The chalcopyrite structure corresponds to phase of the Cu – In – Se system. **Figure II.4** shows ternary phase [30] of this system at room temperature as well as the pseudo-binary diagram $Cu_2Se - In_2Se_3$ [31].

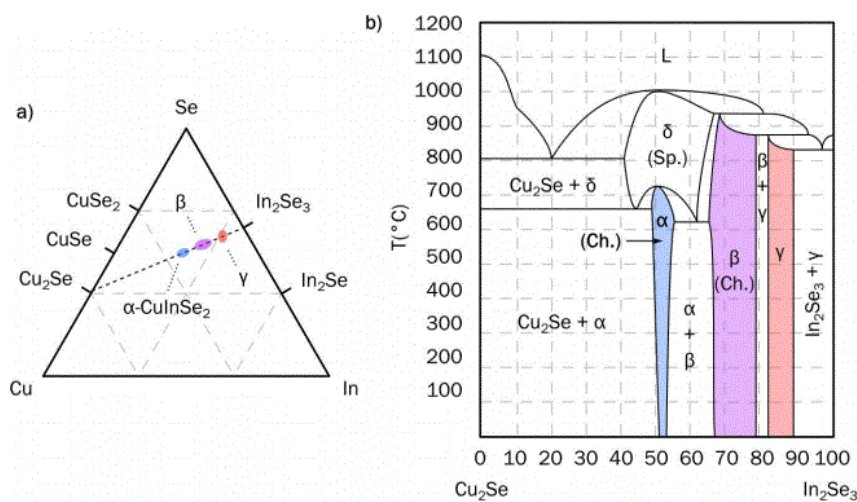


Figure II.4: a) Ternary diagram of the Cu-In-Se system at room temperature .b) Pseudo-binary diagram of the intermediate compounds Cu_2Se and In_2Se_3 [26].

The majority phases obtained during the elaboration of CIS (including the chalcopyrite structure α -CIS), are located around the junction line between these last two compounds [32]. Knowing that the selenium is generally brought in excess during the processes of elaboration of CIS, it is

essentially the ratio of Cu (ratio [Cu]/ [In]) which determines the position (and thus the type of phases formed) on this axis. At ambient temperature, the α -CIS phase corresponds to a Cu concentration of between 24% and 24.5 atomic%. This domain extends as the temperature increases up to about 600° C. Above 700 ° C, a disordered phase of the sphalerite type (δ -CIS) appears. This latter differs from the chalcopyrite phase in that the cation sites are randomly occupied by **Cu** or **In**. This means that in the exact proportions corresponding to the stoichiometric of **CuInSe₂** (25% Cu), a mixture of α -CIS and Cu, was obtained [33]. The same is true for higher copper levels. This configuration is not desirable to realize photovoltaic devices, because the presence of **Cu_{2-x}Se** conductive phase's type in CIS grain boundaries may be the source of short circuits [34].

The phase γ has a flap structure [35]. The phase domain β is in the presence of ordered defects in the α – CIS chalcopyrite structure. This is why these phases are commonly called "ODC phases" (Ordered Defect Compound) has been theoretically demonstrated that these ordered defects are mostly neutral assemblies of the type ($2V_{Cu}^- + In_{Cu}^{2+}$) (two Cu(I) vacancies and substitution of Cu(I) atom by In(III) atom), because their formation is energetically favorable. Be considered as periodic repetitions of a defect ($2V_{Cu}^- + In_{Cu}^{2+}$) all the elementary n cells of α -CIS. The calculations show that the compensation of the In_{Cu}^{2+} by the V_{Cu}^- makes the material less susceptible to the presence of ($2V_{Cu}^- + In_{Cu}^{2+}$). We will see later that these defects, and more particularly the V_{Cu} , participate in the p doping of CIGS [36]. For these reasons, the CIGS is considered a material with a high capacity to remain stable over wide composition ranges, essentially in the Cu-poor domain (copper content below 25%).

II.4 Semiconductor Properties and Gap Adjustment

The semiconducting properties of I–III–VI₂ compounds depend on their composition. The system of copper chalcopyrite $Cu(In, Ga, Al)(Se, S)_2$ includes a wide range of band-gap energies E, from 1.04 eV in $CuInSe_2$ up to 2.4 eV in $CuGaS_2$ and even 2.7 eV in $CuAlS_2$, thus, covering most of the visible spectrum. All these compounds have a direct band gap making them suitable for thin film photovoltaic absorber materials. Thus, substitution of indium with gallium, and / or selenium with sulfur makes it possible to increase the width of the forbidden band. The diagram, shown in “**Figure II.7**”, shows the change in band gap as a function of the mesh parameter for solid solutions ($CuInSe_2$, $CuGaSe_2$, $CuInS_2$ and $CuGaS_2$). This diagram shows that it is easy to modulate the band gap between 1.0 and 2.4 eV by varying the composition of the $Cu(In_{(1-x)}Ga_x)Se_{1-y}S_y$ solid solution [3, 37].

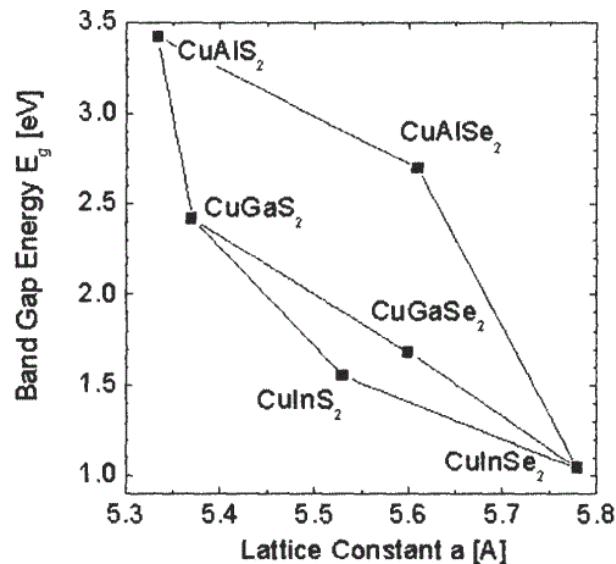


Figure II.5: E_g band-gap energies vs. a lattice constant of the $Cu(In, Ga, Al)(S, Se)_2$ alloy system [3].

The ternary $CuInS_2$ and $CuGaSe_2$ have one width of band gap equal to 1.53 and 1.67 eV, respectively. These two values are close of the value optimal theoretical for one conversion optimal of spectrum solar, equal to 1 of yields of conversion equal to 11.4% for the $CuInS_2$ [38] and 9.7% for the $CuGaSe_2$ [39]. These results are far of best cells of $Cu(In, Ga)Se_2$ for which of yield of conversion of 1 'order of 20% are obtained [40], [41], and [42]. Many studies have shown that the best yields were obtained by increase of the width of band gap at level of interfaces before and back of CIGS (interfaces $CdS / CIGS$ and $Mo / CIGS$. This double gradient of width of band gap can to be obtained by increase of rate of gallium to the face back of CIGS and increase of rate of gallium or of sulphide to the face before, according to the deposition method.

II.5 Electrical properties

Several researchers have studied the electrical properties of $CuInSe_2$, including the identification and characterization of defects in this material. As we mentioned before, we can obtain with this semiconductor a homo- junctions and heterojunctions. On the other hand, this material can presuppose a conductivity of type n or p and this by excess or lack of selenium.

In other words, the $CuInSe_2$, has excellent electrical stability in a wide band of stoichiometry.

Researches have shown that by acting on the ratios $\left(\frac{\text{Cu}}{\text{In}}\right)$ and $\left(\frac{\text{Se}}{\text{Cu} + \text{In}}\right)$ we can change the type of conduction in the CuInSe_2 semiconductor.

Table II.2 brings together the conduction types evolution of the CuInSe semiconductor, as a function of the ratios $\left(\frac{\text{Cu}}{\text{In}}\right)$ and $\left(\frac{\text{Se}}{\text{Cu} + \text{In}}\right)$ after deposition.

Other studies have shown that generally the selenium atoms in **CuInSe** behave like donors and thus lead to n- type conduction. The **CuInSe** layers which have an excess of indium and which contain copper vacancies are generally p-type [43].

Table II.2: Conduction type in CIS in function to the ratio $\left(\frac{\text{Cu}}{\text{In}}\right)$ and $\left(\frac{\text{Se}}{\text{Cu} + \text{In}}\right)$ [43].

$\left(\frac{\text{Se}}{\text{Cu} + \text{In}}\right) > 1$		$\left(\frac{\text{Se}}{\text{Cu} + \text{In}}\right) < 1$	
$\left(\frac{\text{Cu}}{\text{In}}\right) > 1$	$\left(\frac{\text{Cu}}{\text{In}}\right) < 1$	$\left(\frac{\text{Cu}}{\text{In}}\right) > 1$	$\left(\frac{\text{Cu}}{\text{In}}\right) < 1$
Type p with a low resistivity	Type p with a medium resistivity or type n with a high resistivity	Type p with a low resistivity	Type p with a medium resistivity or type n with a high resistivity

II.6 Optical properties of CuInSe_2

The efficiency of solar cells depends mainly on the light absorbed by the absorbing layer. From a technological point of view, the absorbent layer must have an optimal gap to absorb the widest range of wavelengths of the solar spectrum with a high absorption coefficient. The optical properties of the CuInSe_2 layers; have been widely studied by several research groups [44].

CuInSe_2 is distinguished from other photovoltaic materials (CdTe, GaAs, CdS, etc.) by a very high absorption coefficient, greater than 10^5cm^{-1} in the visible range and the infrared p (**Figure II.6**). In addition, CuInSe_2 has a band gap with a direct transition of 1.04 eV [43].

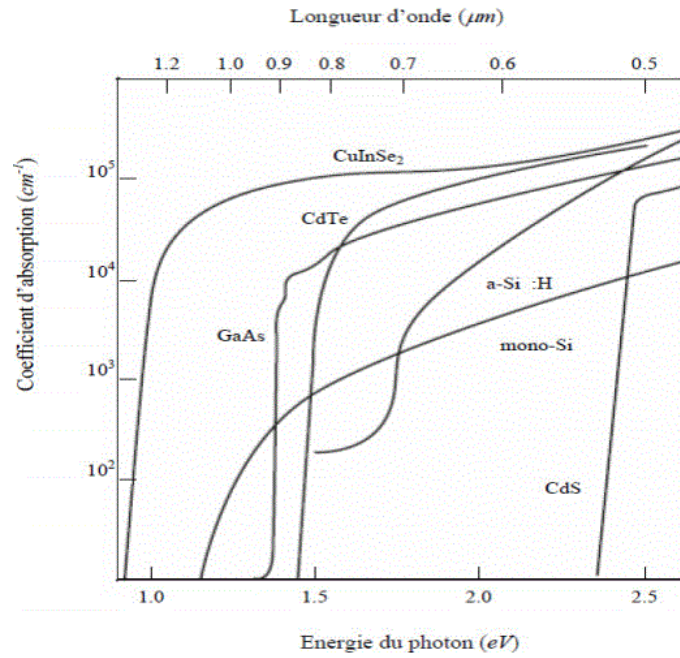


Figure II.6: Absorption's coefficient of materials (CuInSe, CdTe, GaAs, a – Si: H, mono Si and CdS) for the manufacture of cells solar in thin films [44].

In many studies, it was found that the relation between the optic gap E_g and the coefficient of absorption α has for one semiconductor typical is as follows [45]:

$$\alpha = \frac{A(E-E_g)^{1/2}}{E} \quad \text{II.1}$$

With A, a proportionality constant, which depends on the densities states related to photon absorption and E irradiation energy. We can obtain an optical gap with a value: $E = 1.02 \pm 0.02$ eV.

The optical gap of CuInSe is a function also of the temperature, the relation proposed by Varshni [46] can describe it approximately:

$$E_0 - E_g(T) = \left(\frac{\delta T^2}{T + \beta} \right) \quad \text{II.2}$$

Where E_0 is the gap at $0K^0$ and β is a parameter of the same order as the Debye temperature θ_d .

II.7 The structure of CIGS based solar cells

In its most widespread configuration, a CIGS cell is formed of a stack of several thin-film materials deposited successively on a substrate. The latter is usually a soda-lime glass plate (Soda-Lime Glass, SLG). **Figure II.7** shows the standard structure of a CIGS-based cell [26].

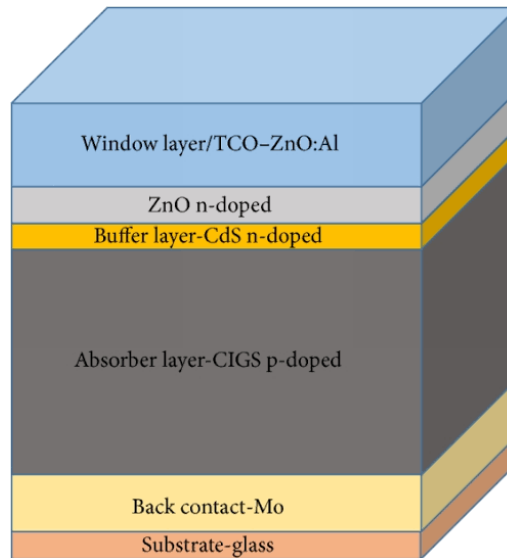


Figure II.7: Standard structure of CIGS based solar cells.

II.8 The layers constitute the CIGS based solar cell

II.8.1 The substrate

The choice for the substrate material is Soda-Lime Glass, which is used in conventional windows. It is the most common substrate material used for $\text{Cu}(\text{InGa})\text{Se}_2$ since it is available in large quantities at low cost and has been used to make the highest efficiency devices. It is an inexpensive substrate material, and offers good resistance to corrosion. It is also easily available at local hardware stores. There are other advantages associated with the use of glass as the substrate, such as the substrate can be used as a packaging material. This becomes even more important when the solar cells are superstrate type, where the light is shone through the glass to reach the absorber. Another benefit of using soda-lime glass is the diffusion of sodium (Na) from the glass to the deposited layers [26, 37].

II.8.2 The Back Contact

The first layer filed on the substrate is the electrode of back contact. It is for a main role of collect the charges generated in the cell. In the electric point of view, it constitutes the anode of

photovoltaic generator. This layer is composed of Molybdenum (Mo) which is a refractory metal that has been widely used as a contact material for $CuInSe_2$ type solar cells. It forms a good ohmic contact, and has a high resistance to selenium corrosion. Its thickness is around 300 nm to 1000 nm. The most deposition method used for the back contact is the magnetron sputtering or DC-plasma [47, 48]. The main properties of the Mo thin films, which make it a proper back contact material for CIGS based solar cells, are:

- Inertness during deposition of the CIGS absorber layer.
- Formation of an ohmic contact.
- Low recombination rate for minority carriers.
- Relative stability at the processing temperature.
- Low contact resistance to CIS and its alloys.
- Resistance to alloying with Cu and In [49].

II.8.3 The CIGS absorber material

Absorber layer is sandwiched between the buffer layer and the back contact [50]. It is the first part of the p-n heterojunction of the cell in which the photons will be converted into electron-hole pairs. In the present case, it is a P-type semiconductor of the I-II-VI family, the various variants that have already been studied lead to the following general formula $(Cu, Ag)(In, Ga, Al)(Se, S, Te)_2$. The substitution of Cu by silver, indium by gallium or aluminum, or selenium by sulfur or tellurium, makes it possible to modify the properties of the material such as its band gap width. The most developed compounds in research and industry are $Cu(In, Ga)Se$ and $Cu(In, Ga)(Se, S)$ [37]. Its thickness is about 1 to 2 μm . The CIGS deposition methods are variable, the most common being the co-evaporation. Beside selenisation and co-evaporation, other deposition methods have been studied, either to obtain films with very high quality or to reduce the cost of film deposition on large areas, methods that are used to grow epitaxial compound films, such as molecular beam epitaxy (MBE) or metal organic chemical vapor deposition (MOCVD)[26].

II.8.4 The buffer layer

The p-n heterojunction with the CIGS is formed by adding a layer called "buffer layer". It plays a role of physical protection of the CIGS during the sputtering deposition of the following layers against damages, and chemical reactions resulting from subsequent deposition steps. Currently,

the best yields are obtained by using buffer layers based on cadmium sulphide (CdS). In addition, it is the most used material. However, due to the toxicity of cadmium, significant efforts are directed towards the development of alternative buffer layers (Zn (O, S), (Zn, Mg)O, $\text{In}_2(\text{S,Se})_3$ etc.). The typical thickness of a CdS buffer layer is about 50 nm. The most common method of depositing CdS is the Chemical Bath Deposition (CBD) [26].

II.8.5 The window layer

The buffer layer is covered with a window layer. This layer composed of a deposit zinc oxide (ZnO) and a transparent conductive oxide (TCO). This layer is resistive and serves to limit the formation of short circuits in areas with perfect recognition of the CIGS by the buffer layer. The most widely used TCOs are ZnO doped aluminum (ZnO: Al) and indium tin oxide (ITO) deposited by sputtering. The TCO allows the window layer to form contact part before the photovoltaic cell while being transparent to solar radiation, the latter to be absorbed in the CIGS layer. The thickness of the window layer is of the order of 300 nm to 500 nm [26].

II.8.6 The front contact

The final front contact is made by adding to the stack a grid, which will collect the charges generated by the cell. This grid consists of a layer of nickel and an aluminum layer. Ni serves as a tie layer and avoids the oxidation of Al due to the underlying presence of TCO. The grids are generally deposited by evaporation using a deposition mask [26].

Figure II.8 show the band diagram of a CIGS/CdS/ZnO solar cell.

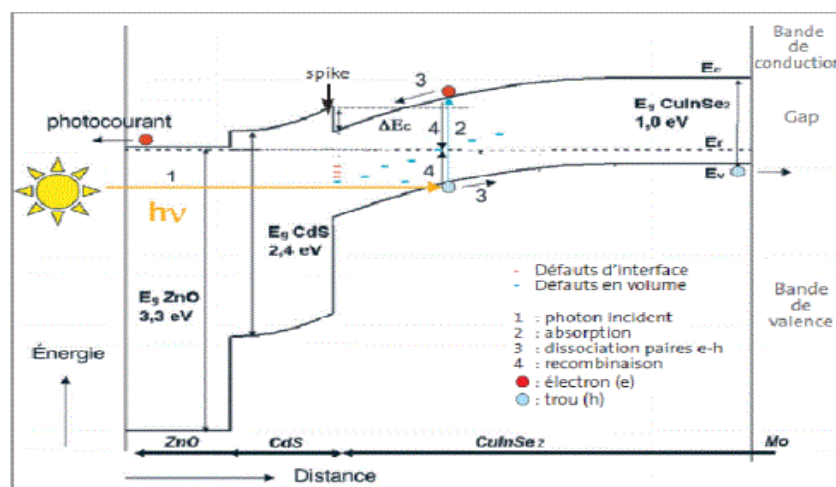


Figure II.8: Bands diagram of a CIGS/CdS/ZnO cell.

At the interface CIGS/CdS, neighbourhood, energy bands are curved by the variation of electrostatics potential through the p-n junction. The interface between CIGS and CdS present one discontinuity of positive energy at the conduction band level and this discontinuity must possess one height optimal for the performance of devices too high, it precludes at passage of photo-generated electrons reducing the photo-current; too low, even negative, she increases the darkness current and the losses by recombination. The intrinsic layer of ZnO complete the buffer layer on the electric plan, in avoiding the direct contact with ZnO: Al which is electrically degenerate. Due to the high band gap widths fact, visible radiation which is then absorbed into the CIGS layer. The characteristics of the cells will therefore ultimately depend closely on those of the individual layers and their interfaces. The increase, for example, of the band gap of the CIGS will be accompanied by an increase in the open circuit voltage at the expense of the photocurrent. Unlike silicon cells, this is a heterojunction device. The photocurrent is generated in CIGS layer and then passes through CdS / ZnO layers, unlike silicon where the n layer contributes to the photocurrent. The advantage of the heterojunction is to limit the optical losses in the n zone of a classic homojunction.

The efficiency of CIGS based solar cells depends on the properties of the absorber material. As in the case of other semiconductor, the crystalline structure of CIGS as well as its composition can strongly influence on its optical and electronics properties. The good understanding of the structure of this material is therefore necessary in the purpose of optimizing the basic CIGS device.

II.9 The performance of a $CuInSe_2$ based solar cell

The efficiencies of the solar cells based on the absorber $CuInSe_2$ are summarized in “Table II.3”. In most cases, the high efficiencies are obtained for laboratory photovoltaic cells of very small size ($<1cm^2$). The increase of the open circuit voltage and the decrease of the current density which would result, a reduction in the number of interconnections and, on the other hand, would avoid the use of highly conductive transparent oxide layers, and efficiency losses would be less pronounced as a function of temperature, which is a competitive advantage in applications.

The development of bit higher gap materials is of particular interest The widening of the forbidden band by the introduction of a high rate of Ga in the $CuInSe_2$ is only possible in the case of evaporation process , because one always finds a segregation of the Ga towards the back

contact in the process of selenization. CuInS , having a gap of 1.5 eV, is perceived by a part of the community as particularly interesting for a more ecological production of cells where selenium is replaced by sulfur. In both processes (sequential and co-evaporation), a good homogeneity is obtained because the material is hard prepared in Cu and the stoichiometric is obtained by a self-adjusting chemical attack [51].

Table II.3: The efficiency of $\text{Cu(In, Ga)(S, Se)}_2$ absorbers based photovoltaic cells.

Solar cell types	Efficiency (%)
$\text{CuInSe}_2/\text{CdS}/\text{ZnO}/\text{MgF}_2$	14.8
$\text{Cu(In, Ga)Se}_2/\text{CdS}/\text{ZnO}/\text{MgF}_2$	18.8
$\text{Cu(In, Ga)Se}_2/\text{CdS}/\text{ZnO}/\text{MgF}_2$	17.7
$\text{Cu(In, Ga)Se}_2/\text{CdS}/\text{ZnO}/\text{MgF}_2$	17.6
$\text{CuInSe}_2/\text{CdS}/\text{ZnO}/\text{MgF}_2$	12
$\text{CuIn}_{1-x}\text{Ga}_x\text{Se}_2$	19.2
$\text{Cu(In, Ga)Se}_2/\text{CdS}/\text{ZnO}/\text{MgF}_2$	19.3
$\text{Cu(In, Ga)Se}_2/\text{CdS}/\text{ZnO}/\text{MgF}_2$	20
$\text{Cu(In, Ga)(S, Se)}_2$	20

The chalcopyrite family is also particularly attractive because it offers gap semiconductors ranging from 1 to 2.4 eV. This suggests the development of multispectral photovoltaic cells capable of making the most of the components of the solar spectrum. In addition, high yields are obtained by combining CuGaSe_2 and CuInSe_2 in a tandem structure. Note that an efficiency of 33.9% is obtained for a CGS / CIS tandem for illumination of AM1.5 [51].

II.10 Features and disadvantages

II.10.1 Features

- ✓ CIS and CIGS cells are low-cost than wafer- based crystalline silicon modules.
- ✓ Little defects due to the low temperature of annealing, thus the propagation length is relatively long.

- ✓ Copper indium diselenide and related materials. Copper indium diselenide (CIS) and copper indium gallium diselenide (CIGS) are direct gap polycrystalline semiconductor that can be setting to match the solar spectrum by replacing indium with Ga.
- ✓ High optical absorption coefficients (10^5 cm^{-1}) so the CIGS thickness can be about 100 times less than the thickness of the c-Si wafer ($1 \mu\text{m}$ - $2.5\mu\text{m}$) is sufficient for the device.
- ✓ The CIGS material can be deposited on rigid as well as flexible substrates.
- ✓ The conductivity can be controlled by changing the ratio of In with Ga.
- ✓ CuInSe_2 is a self-doped (intrinsically doped) material, which means that, when the compound is formed, it automatically becomes either p- or n-type, depending in the composition [47, 48, 49].

II.10.2 Disadvantages

- It has a problem of instability in a hot and humid environment.
- CIS and CIGS are always used in a heterojunction structure, mostly with very thin n-type cadmium sulfide (CdS) layers but the Cd is toxic element.
- In and Ga are rare and expensive items. The availability of indium in Earth's crust is comparable to that of silver, and because of this relative scarcity, indium has been subject to erratic fluctuations in world market price.
- The back contact is very limited, molybdenum is mostly only used or molybdenum oxide (MO_x) however the homojunction obtained not well [47, 48].



CHAPTER III:

SCAPS software

(Solar cell

CAPacitance

Simulator)



III.1 Introduction

SCAPS is a one-dimensional solar cell simulation program developed at the department of Electronics and Information Systems (ELIS) of the University of Gent, Belgium. Several researchers have contributed to its development: Alex Niemegeers, Marc Burgelman, Koen Decock, Johan Verschraegen, Stefaan Degraeve. A description of the program, and the algorithms it uses, is found in the literature. The program is freely available to the PV research community (universities and research institutes). It runs on PC under Windows 95, 98, NT, 2000, XP, Vista, Windows 7, and occupies about 50 MB of disk space. SCAPS is originally developed for cell structures of the CuInSe₂ and the CdTe family. Several extensions, however, have improved its capabilities so that it is also applicable to crystalline solar cells (Si and GaAs family) and amorphous cells (a-Si and micro-morphous Si). An overview of its main features is given below [52, 53]:

- Up to 7 semiconductor layers.
- Almost all parameters can be graded (i.e. dependent on the local composition or on the depth in the cell) : $E_g, \chi, \varepsilon, N_V, N_C, v_{thn}, v_{thp}, \mu_n, \mu_p, N_A, N_D$ all traps (defects) N_T .
- Recombination mechanisms: band-to-band (direct), Auger, SRH-type.
- Defect levels: in bulk or at interface; their charge state and recombination is accounted for.
- Defect levels, charge type: no charge (idealisation), monovalent (single donor, acceptor), divalent (double donor, double acceptor, amphoteric), multivalent (user defined).
- Defect levels, energetic distributions: single level, uniform, Gauss, tail, or combinations.
- Defect levels, optical property: direct excitation with light possible (impurity photovoltaic effect, IPV).
- Defect levels, metastable transitions between defects.
- Contacts: work function or flat-band; optical property (reflection of transmission filter) filter.
- Tunneling: intra-band tunneling (within a conduction band or within a valence band); tunneling to and from interface states.
- Generation: either from internal calculation or from user supplied $g(x)$ file.
- Illumination: a variety of standard and other spectra included (AM0, AM1.5D, AM1.5G, AM1.5G edition2, monochromatic, white, etc...).
- Illumination: from either the p -side or the n -side; spectrum cut-off and attenuation... and many other characteristics detailed in the software manual.

III.2 The basics

SCAPS is a Windows-oriented program, developed with Lab Windows/CVI of National Instruments. We use here the LW/CVI terminology of a ‘Panel’ (names used in other software’s are: a window, a page, a popup...). SCAPS opens with the ‘Action Panel’ [53].

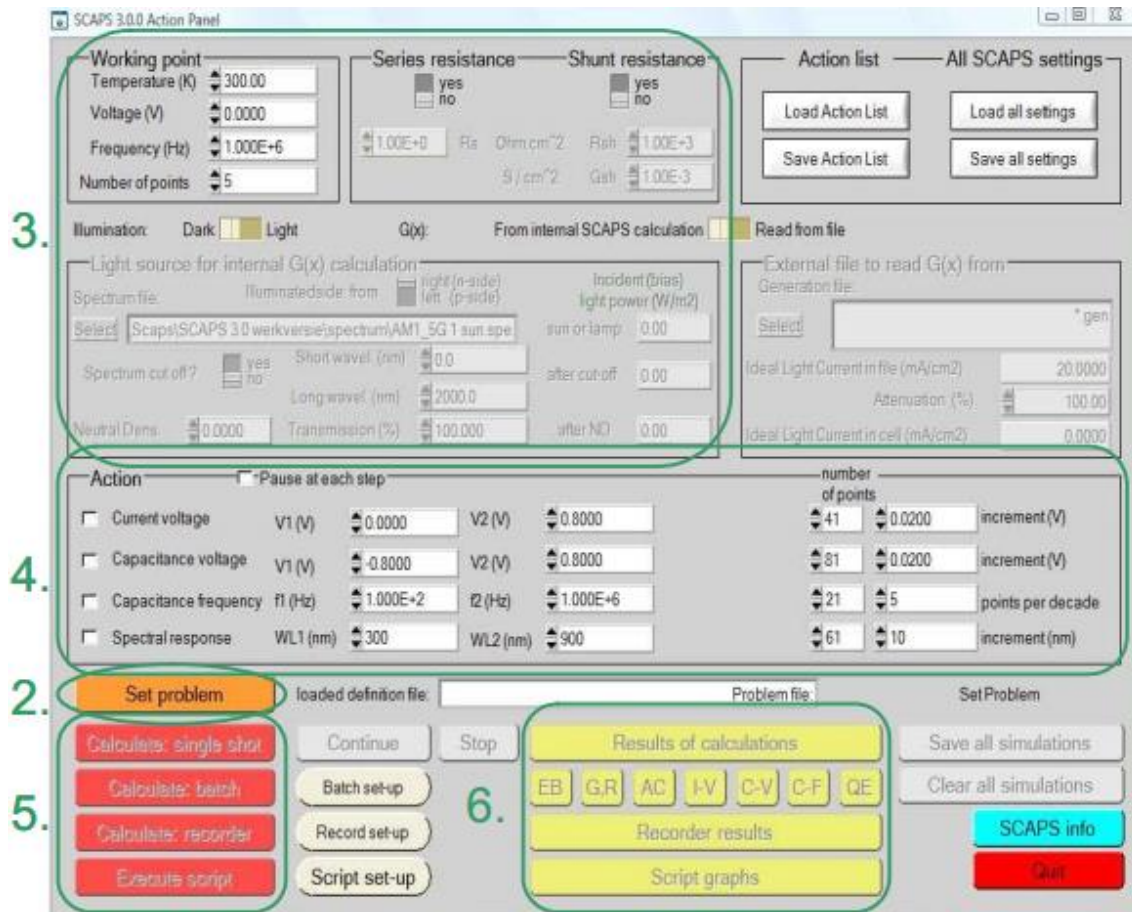


Figure III.1: The SCAPS start-up panel, the Action panel or main panel.

There are dedicated panels for the basic actions:

1. Run SCAPS.
2. Define the problem, thus the geometry, the materials, all properties of your solar cell.
3. Indicate the circumstances in which you want to do the simulation, i.e. specify the working point.
4. Indicate what you will calculate, i.e. which measurement you will simulate.
5. Start the calculation(s).
6. Display the simulated curves. This is further explained below.

III.2.1 Run SCAPS

Click the below pictogram on the Desktop, or double-click the file SCAPS3200.EXE in the file manager (or any other SCAPS version). SCAPS opens with the Action Panel [53].



III.2.2 Define the problem

Click the button SET PROBLEM in the action panel (**Figure III.2 (a)**), and chose LOAD in the lower right corner of the panel that opens. Select and open e.g. the file NUMOS CIGS baseline.def: that is the example problem file of CIGS based solar cells. In a later stage, you can modify all properties of the cell by clicking SET PROBLEM in the action panel [52, 53, 54].

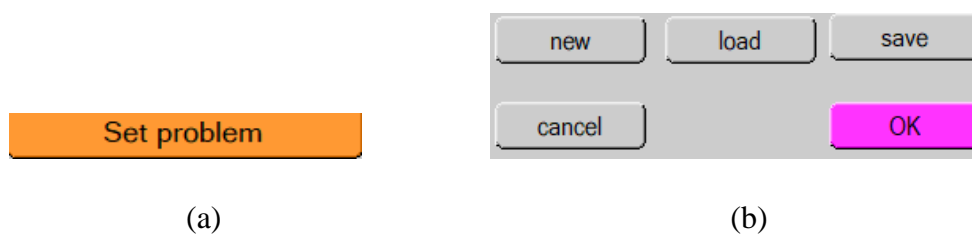


Figure III.2: Define the problem.

III.2.3 Define the working point

The working point specifies the parameters which are not varied in a measurement simulation, and which are relevant to that measurement. Thus [53]:

- The temperature T : relevant for all measurements. Note: in SCAPS, only $N_c(T)$, $N_v(T)$, the thermal velocities, the thermal voltage KT and all their derivatives are the only variables, which have an explicit temperature dependence; you must input for each T the corresponding materials parameters yourself.
- The voltage V : is discarded in I - V and C - V simulation. It is the DC bias voltage in C - f simulation and in $QE(\lambda)$ simulation. SCAPS always starts at 0V, and proceeds at the working point voltage in a number of steps that you also should specify.
- The frequency f : is discarded in I - V , $QE(\lambda)$ and C - f simulation. The C - V measurement is simulated at a given frequency.

• The illumination: is used for all measurements. For the $QE(\lambda)$ measurement, it determines the bias light conditions. The basis settings are dark or light, choice of the illuminated side, choice of the spectrum. A one sun ($= 1000 W / m^2$) illumination with AM=1.5 global spectrum is the default, but you have a large choice of monochromatic light and spectra for your specialized simulations. If you have an optical simulator at your disposal, you can immediately load a generation profile as well instead of using a spectrum.

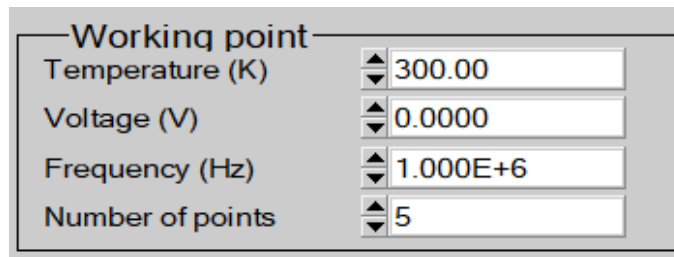


Figure III.3: The working point.

III.2.4 Select the measurement(s) to simulate

In the action-part of the Action Panel, you can select one or more of the following measurements to simulate I - V , C - V , C - f and $QE(\lambda)$.

Adjust if necessary the start and the end values of the argument, and the number of steps. Initially, do one simulation at a time, and use rather coarse steps: your computer and/or the SCAPS program might be less fast than you hope, or your problem could be tough... A hint: in a C - V simulation, the I - V curve is calculated as well; no need then to specify it separately [53, 54].

III.2.5 Start the calculation(s)

Click the button CALCULATE: SINGLE SHOT in the action panel “Figure III.4”. The Energy bands panel opens, and the calculations start. At the bottom of the panel, you see a status line, e.g. “IV from 0.000 to 0.800 Volt: $V = 0.550 Volt$ ” showing you how the simulation proceeds. Meanwhile, SCAPS stands you a free movie how the conduction and valence bands, the Fermi levels and the whole caboodle are evolving. When you see the hated divergence message, you are entitled to get into a bad mood, but do not exaggerate. Anyway, you did not lose the I - V points already calculated [52, 53].

Calculate: single shot

Figure III.4: Calculate single shot.

III.2.6 Display the simulated curves

After the calculation(s), SCAPS switches to the Energy band panel (or the AC-band panel). You can now look at your ease to the band diagrams, carrier densities, and current densities; at the last bias point calculated. You can output the results (buttons print, save graphs, show (then the numbers are shown on screen; cut & paste to e.g. Excel is possible), or save (then the numbers are saved to a file). You can switch to one of the specialized output Panels (if you have already simulated at least one corresponding measurement). We only show the example of the IV Panel [52, 53].

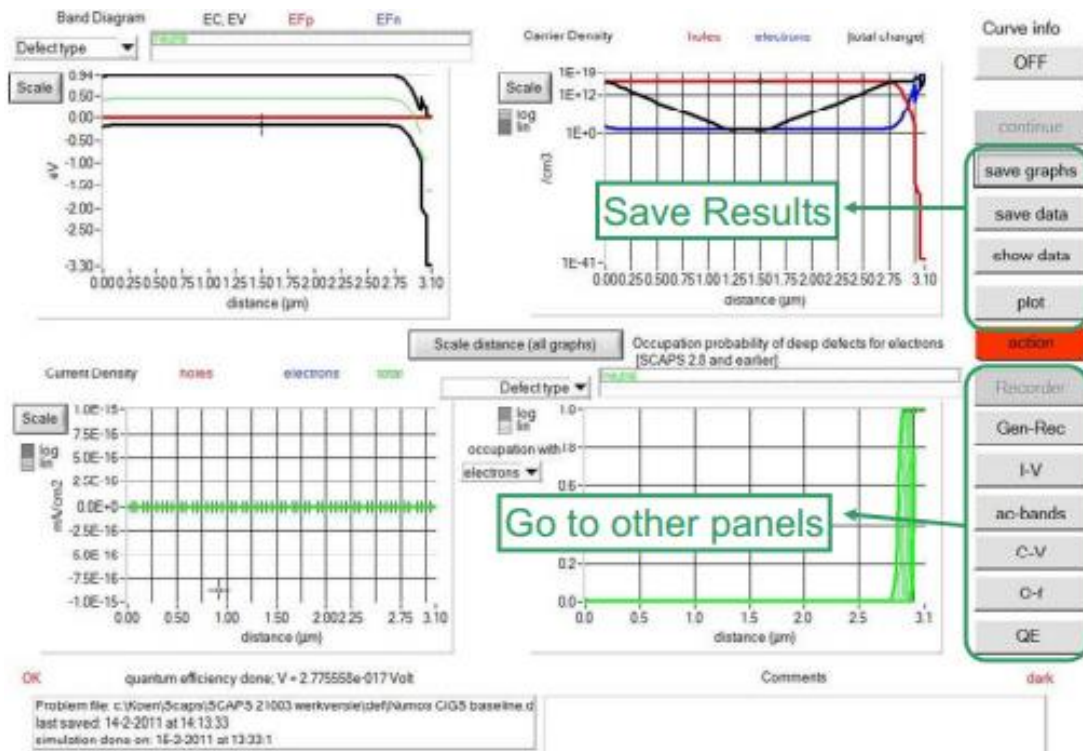


Figure III.5: The energy band panel.

III.2.7 The I-V curves

The meaning of the PLOT, SHOW or SAVE buttons is as for the Energy Bands Panel. Again, you can switch to the other output panels (energy bands, AC, C-V, C-f and QE, if already calculated), and to the Action Panel to do a new calculation or to stop (important: you can only

leave SCAPS from the Action Panel). Several small remarks: The color of the last calculated curve is indicated (tip: when the graph gets too crowded, go to the Action Panel and click clear all simulations to clear all graphs). The recombination curves are only shown for the last simulation. The color of the legend corresponds to the color of the curve (indicated as 1bis). If Curve Info is switched ON and you click the cursor on a curve in a graph, a pop-up panel will appear which gives information about the graph, curve and the point that you clicked [53].

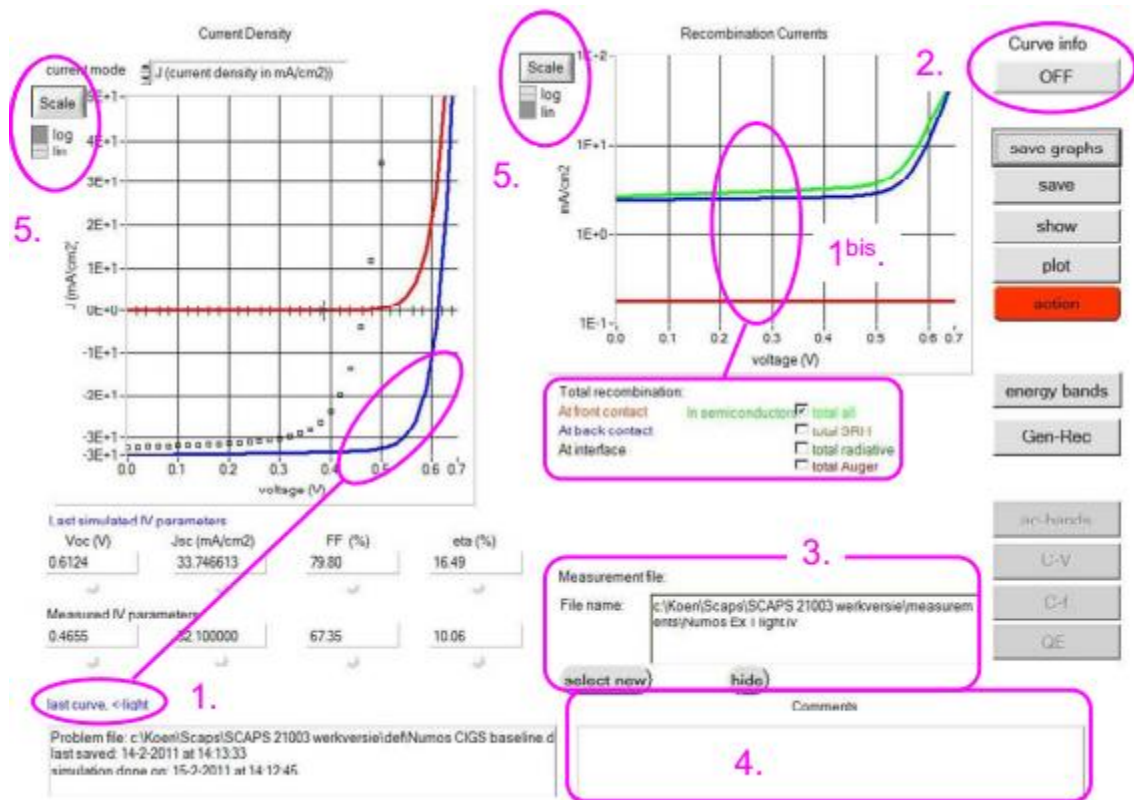


Figure III.6: I-V curve display panel in the dark and in light.

You can change the range and scaling of the axes with the SCALE button. If you press the CTRL button and select a rectangular area in a graph, the graph will zoom-in to the selected area. Pressing the CTRL button and clicking the right mouse button results in zooming out [53].

III.3 Solar cell definition

The recommended way to introduce your solar cell structure into SCAPS is to use the graphical user interface. This way you can interactively set all parameters while SCAPS watches over you, so that you do not define impossible or unrealistic situations. This chapter explains which situations can be modelled and how to introduce them in SCAPS [53, 54].

III.3.1 Edition a Solar cell structure

When clicking the ‘Set Problem’-button on the action panel, the ‘Solar cell definition’-panel is displayed. This panel allows to create solar cell structures and to save those to or load from definition files. These definition files are standard ASCII-files with extension ‘*.def.’ which can be read with e.g. notepad. Even though the format of these files seems self-explaining, it is however strongly disadvised to alter them manually. Layer-, contact-, and interface properties can be edited by clicking on the appropriate box as shown in Figure In a similar way, layers can be added by clicking ‘add layer’[53, 54].

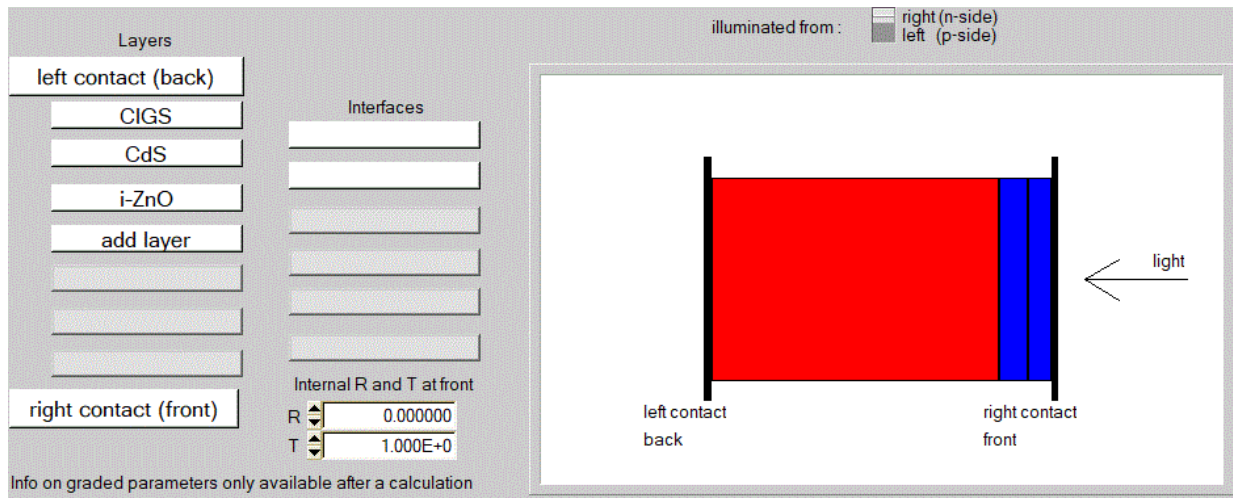


Figure III.7: Defining a solar cell structure.

III.3.2 Contacts

The contact properties can be set by either clicking the front or back contact button on the cell definition panel, which opens the ‘contact properties panel’, **Figure III.8** [53].

The screenshot shows the 'Contact properties' panel, divided into two sections: 'Electrical properties' and 'Optical properties'.

Electrical properties:

- Thermionic emission / surface recombination velocity (cm/s):
 - electrons: 1.00E+5
 - holes: 1.00E+7
- Metal work function (eV): 5.0000 or flat bands
- Majority carrier barrier height (eV):
 - relative to EF: 0.2000
 - relative to EV or EC: 0.0000
- Allow tunneling
- Effective mass of electrons: 1.00E+0
- Effective mass of holes: 1.00E+0

Optical properties:

- optical filter:
- Filter Mode: transmission, reflection
- Filter Value: 0.700000
- Complement of Filter: 3.0000E-1
- From Value: (light grey bar)
- From File: (dark grey bar)
- Select Filter File:

Buttons: OK (pink), cancel (grey)

Figure III.8: Contact properties panel.

The properties of the contacts are divided into electrical and optical properties. In the electrical properties, we define the surface recombination rates of electrons and free holes. If the contact has an exit job, or it is ideal (flat band scheme). The barrier of the majority carriers. The tunnel effect (if we want to consider it). For optical properties, the transmission or reflection can be defined by a value or a data file.

III.3.3 Definitions of layers

By clicking on the "add layer" button, a window (*Figure III.9*) opens that contains different parameters of the material to introduce. These parameters can have uniform or non-uniform distributions depending on the physics of the material. In the first box, we introduce the name of the layer (which corresponds to the type of doping). Second box, the thickness of the layer

is introduced. The third block, concerns the purity of the material and its profile. In the fourth block, we introduced: the energy gap, the electronic affinity, the dielectric permittivity, the effective densities of the conduction and valence bands, the thermal velocities of the electrons and the free holes, the mobilities of the electrons and holes, a box, which makes it possible to add the effective masses of the electrons and holes if we hold transport carriers by tunnel effect.

If the material is a compound to introduce gradual variations of the previous parameters. In the fifth block, **Figure III.10**, one introduces the doping, type and density. Doping can also be introduced as being uniform, as it can have gradual variations (linear, parabolic ...) and holes. Finally, in the sixth block, account is taken of elements with non-uniform concentrations, and the absorption of the layer is defined, as shown in Figure. The analytical model provided by SCAPS, as it can be introduced as data can define absorption. SCAPS provides a number of absorption data for several types of semiconductors. Other absorption data can also be used for semiconductors not available in SCAPS, if the file has the same extension of the absorption files provided by SCAPS.

The screenshot shows the 'SCAPS 3.2.00 Layer Properties Panel' for 'LAYER 1'. The material is identified as 'CIGS'. The thickness is set to 1.000 μm. The doping profile is 'uniform pure A (y=0)' with a concentration of 0.000. The semiconductor property is 'pure A (y = 0)'. The following physical properties are defined:

bandgap (eV)	1.200	
electron affinity (eV)	4.500	
dielectric permittivity (relative)	10.000	
CB effective density of states (1/cm ³)	2.000E+18	
VB effective density of states (1/cm ³)	2.000E+18	
electron thermal velocity (cm/s)	1.000E+7	
hole thermal velocity (cm/s)	1.000E+7	
electron mobility (cm ² /Vs)	5.000E+1	
hole mobility (cm ² /Vs)	2.000E+1	
<input type="checkbox"/> Allow Tunneling	effective mass of electrons	1.000E+0
	effective mass of holes	1.000E+0

Figure III.9: Properties of the added layer

no ND grading (uniform)	
shallow uniform donor density ND (1/cm ³)	0.000E+0
no NA grading (uniform)	
shallow uniform acceptor density NA (1/cm ³)	5.500E+15

Figure III.10: Properties of defined doping.

Absorption model

alpha (y=0)
 from model
 from file

absorption constant A (1/cm eV ^{1/2})	1.000E+5
absorption constant B (eV ^{1/2} /cm)	0.000E+0

show save absorption file for y = 0

Figure III.11: The absorption model.

The type of volume recombination presents is indicated in the right side of the properties panel of the layer. All types of recombination are present; directly or through the traps.

Recombination model

Band to band recombination

Radiative recombination coefficient (cm ³ /s)	0.000E+0
Auger electron capture coefficient (cm ⁶ /s)	0.000E+0
Auger hole capture coefficient (cm ⁶ /s)	0.000E+0

Defect 1 of CIGS

defect type	Neutral
capture cross section electrons (cm ²)	1.000E-15
capture cross section holes (cm ²)	1.000E-15
energetic distribution	Single
reference for defect energy level Et	Above EV (SCAPS < 2.7)
energy level with respect to Reference (eV)	0.600
characteristic energy (eV)	0.100

Nt grading dependent on position x: Nt (x) uniform

Nt total (1/cm³) Left (x=0) 1.000E+18 Right (x=1) 1.000E+18

Figure III.12: Definition of recombination types.

If we introduce the defects (traps), they may be uniform or non-uniform, discrete, with Gaussian, donor, acceptor, neutral, monovalent or divalent distributions. We can even define carrier transitions between the different energy levels of the traps.



CHAPTER IV:

*Results and
discussion*

IV.1 Introduction

In order to optimize a specific design of a ZnO / CdS / CIGS heterojunction structure, we need to analyze and interpret the results to determine the influence of physical and technological parameters on device performance such as the thickness, the defects, the permittivity...etc. In the following work we will study the effect of the relative permittivity of the three layers CdS ZnO and CIGS in the short circuit current density (J_{sc}), the open circuit voltage (V_{oc}), the fill factor (FF) and the photovoltaic conversion efficiency (η).

This chapter aims to present the numerical simulation results of CIGS based solar cells by SCAPS software by studying the effect of permittivity on the solar cell's figures of merit.

The relative permittivity of the materials constituting heterojunction solar cells is usually not considered as a design parameter when searching for novel combinations of heterojunction materials. In this work, we show the effect of the materials permittivity on the physics and performance of the solar cell by means of numerical simulation. In particular, we argue that high permittivity materials should always be the preferred choice as heterojunction partners of the absorber layer when prototyping new materials combinations. When the heterojunction partner has a high permittivity, solar cells are consistently more robust against several non-idealities that are especially likely to occur in early-stage development, when the device is not yet optimized [6].

IV.2 The structure of the studied solar cell

Our work consists of modeling a CIGS based solar cell and simulating these electrical parameters. In our study, we use a solar cell with CIGS absorbing layer of the following structure: ZnO/CdS /CIGS/Mo. The simplified scheme of the heterojunction structured is shown in “*Figure IV.1*”.

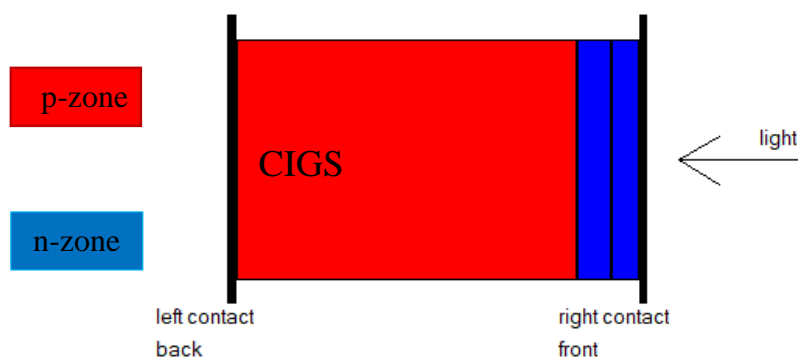


Figure IV.1: Simplified diagram of a solar cell in CIGS thin layer.

IV.3 The studied device parameter

Table IV.1: Properties of the three layers CIGS, CdS, i – ZnO.

Layer properties	CIGS	CdS	i – ZnO
Thickness(μm)	1.000	0.1000	0.080
Band gap (eV)	1.200	2.450	3.400
Electron affinity (eV)	4.500	4.450	4.550
Dielectric permittivity	13.600	10.000	9.000
CB effective density of states (cm^{-3})	2×10^{18}	2×10^{18}	4×10^{18}
VB effective density of states (cm^{-3})	1.5×10^{19}	2×10^{18}	9×10^{18}
Electron thermal velocity (cm/s)	1×10^7	1×10^7	1×10^7
Hole thermal velocity (cm/s)	1×10^7	1×10^7	1×10^7
Electron mobility ($\text{cm}^2/\text{V.s}$)	5000	5000	5000
Hole mobility ($\text{cm}^2/\text{V.s}$)	2000	2000	2000

IV.4 Result and discussion

IV.4.1 The effect of the relative permittivity on CIGS figures of merit

IV.4.1.1 The influence of the relative permittivity of CdS layer

The main function of CdS layer in the structure is to form the heterojunction with the CuInSe₂ layer.

Figure IV.2 represents the change of current density in terms of the voltage and the quantum efficiency of CIGS based solar cells respectively to several values of the relative permittivity of CdS layer.

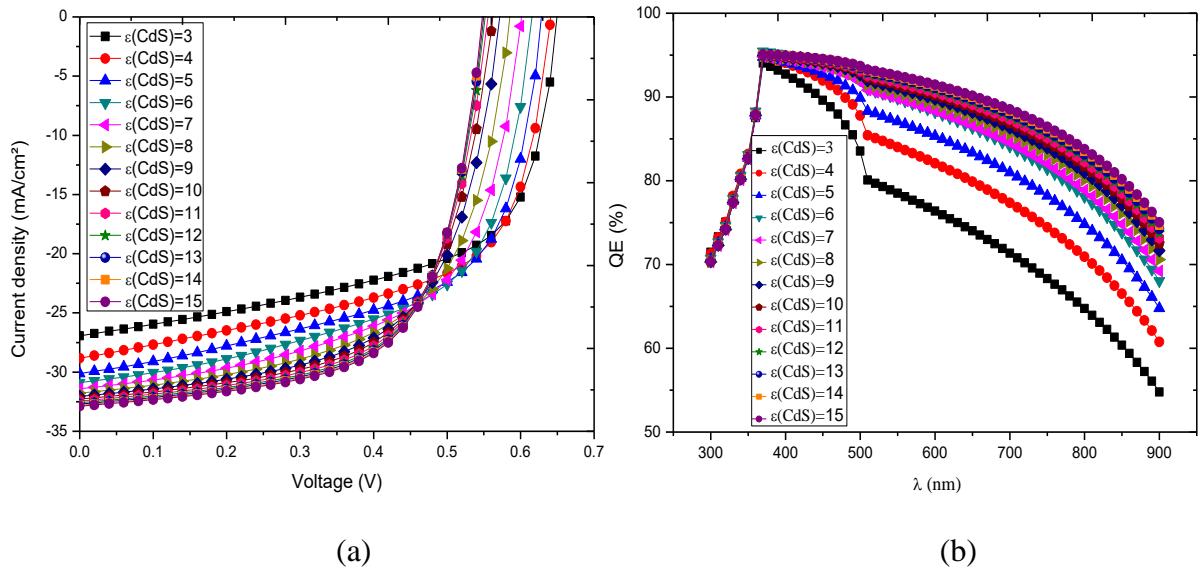
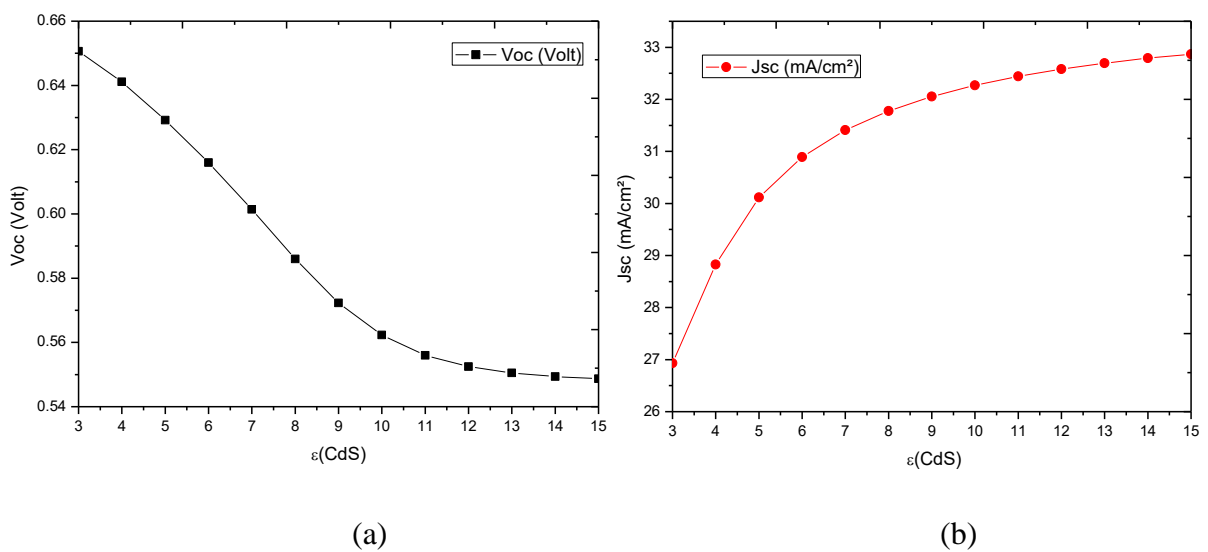


Figure IV.2: (a) The J-V characteristic and (b) the quantum efficiency for CdS layer.

We notice that the current increases when the value of the relative permittivity of the CdS layer increases. The increase in the relative permittivity increases the quantum efficiency, which gives an increase in the number of the generated electrons-holes pairs and thus increase the current. The open circuit voltage decrease for the internal voltage is affected by the increase in the relative permittivity.

Figure IV.3 show the effect of the relative permittivity of CdS layer in: the open circuit voltage, short circuit current density, the fill factor and the efficiency, respectively



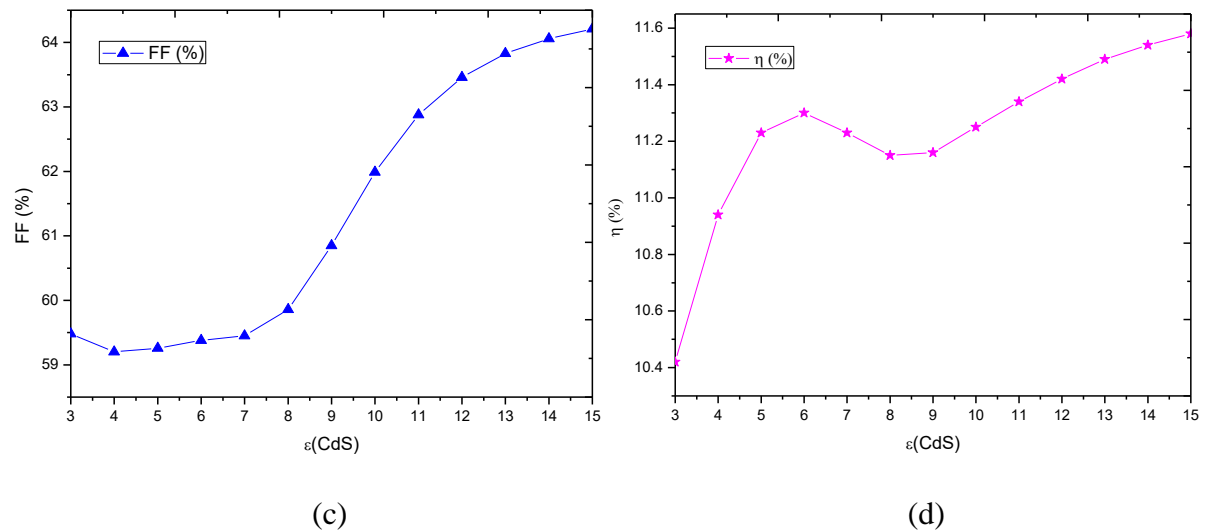


Figure IV.3: The effect of the relative permittivity of CdS layer in: (a) open circuit voltage, (b) short circuit current density, (c) the fill factor, (d) the efficiency.

We notice that the J-V characteristic improves for the big values of the relative permittivity of CdS layer.

We notice that the open circuit voltage decrease slightly from high value (when $\epsilon = 3$; $V_{oc} = 0.6506 \text{ V}$) to a minimum value (when $\epsilon = 15$; $V_{oc} = 0.5487$). The short circuit current increases with the increase of the relative permittivity of the CdS layer. The fill factor in the first (when $\epsilon=3$) has a small value ($FF = 59.48 \%$), and for ($\epsilon = 4$), it decreases to a less value ($FF = 59.20 \%$) and after increases with the increase of the permittivity. This lead to the increase of the quantitative yield, which gives an increase in the number of the generated electrons- holes pairs thus increase the current. The outcome of these changes gives the effect on the solar cell's efficiency that generally increases from 10.42 % to a greater value, which is 11.58 %.

IV.4.1.2 The influence of the relative permittivity of $i - \text{ZnO}$ layer

a) For: $\epsilon_{(\text{CdS})} = 10$, $\epsilon_{(\text{CIGS})} = 13.6$ and $\epsilon_{(\text{ZnO})} = 3 \dots 15$.

Figure IV.4 represents the change of current density in terms of the voltage and the quantum efficiency of CIGS based solar cells respectively to several values of the relative permittivity of ZnO window layer

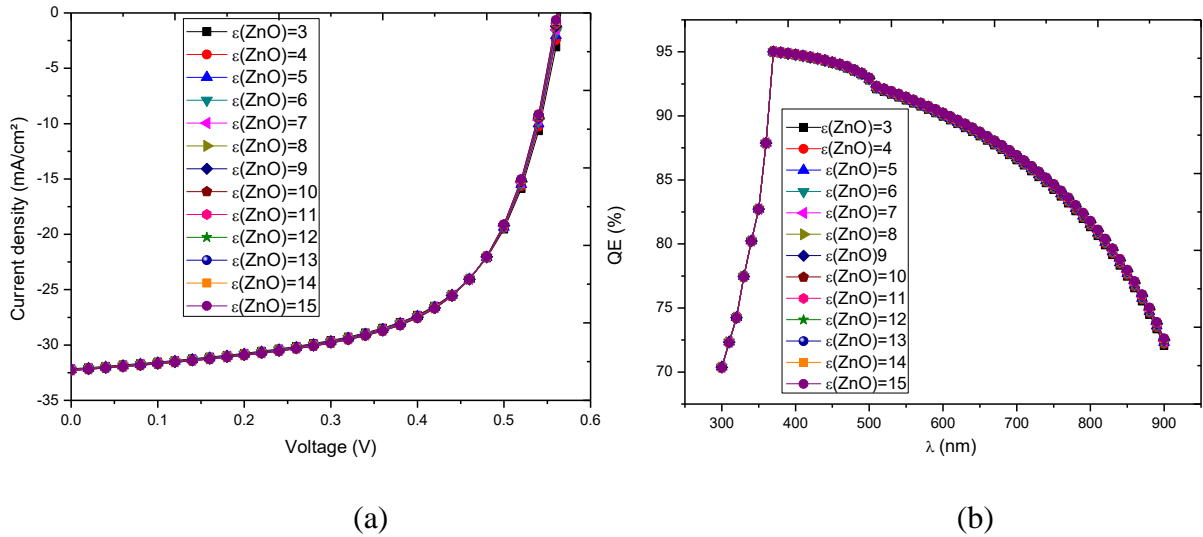
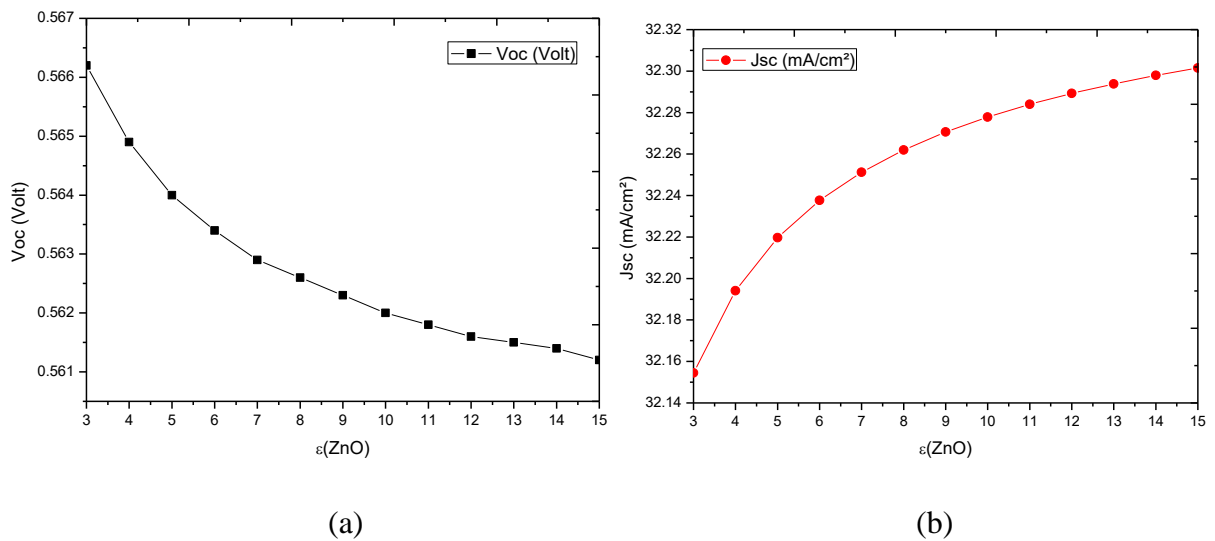


Figure IV.4: (a) The J-V characteristic for ZnO window layer where $\epsilon(\text{CdS}) = 10$ and $\epsilon(\text{CIGS}) = 13.6$, (b) the quantum efficiency.

We notice that the current and the voltage is not affected when the value of the relative permittivity of the ZnO window layer increases. The increase in the relative permittivity is not affect in the quantitative yield, so the number of the generated electrons-holes pairs, thus the current stay constant. The open circuit voltage is constant for the internal voltage not affected by the increase in the relative permittivity.

Figure IV.5 show the effect of the relative permittivity of ZnO window layer in: the open circuit voltage, short circuit current density, the fill factor and the efficiency.respectively



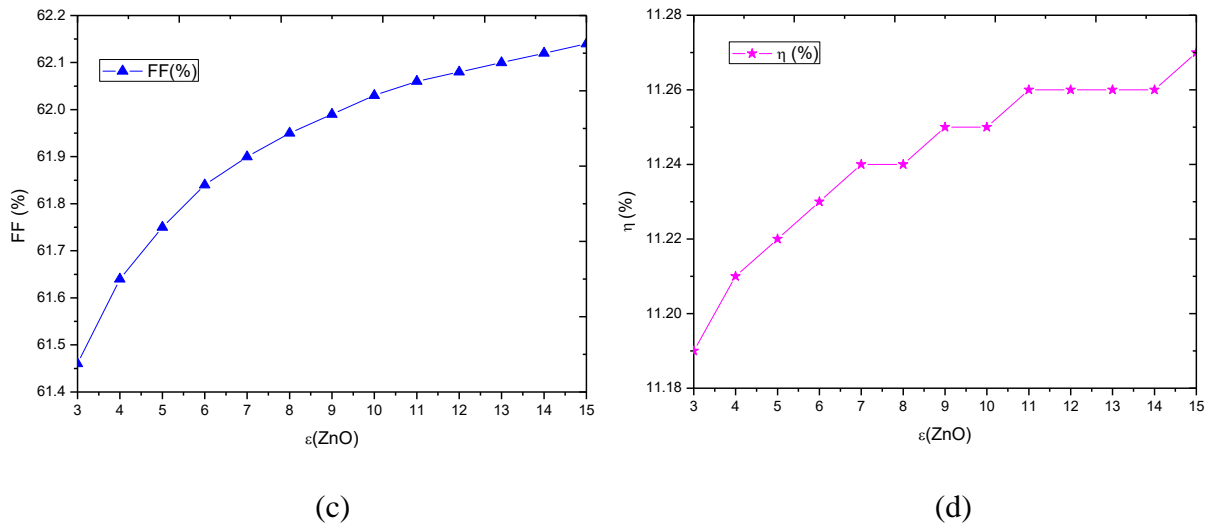


Figure IV.5: The effect of the relative permittivity of ZnO window layer in: (a) open circuit voltage, (b) short circuit current density, (c) the fill factor and (d) the efficiency.

We notice that the J-V characteristic is not affected for the changing in values of the relative permittivity of ZnO window layer.

We notice that the open circuit voltage in the first value ($\epsilon = 3$) has a high value ($V_{oc} = 0.5662 \text{ V}$) and after decreasing slowly to a minimum value ($\epsilon = 15$; $V_{oc} = 0.5612 \text{ V}$). The short circuit current and the fill factor increase with the increase of the relative permittivity of the ZnO window layer. This lead to the outcome of these changes gives the effect on the solar cell's efficiency that increases slightly from 11.19 % to a greater value, which is 11.27 %.

b) For: $\epsilon_{(CdS)} = 15$, $\epsilon_{(CIGS)} = 13.6$ and $\epsilon_{(ZnO)} = 3 \dots 15$.

The same as the “Figure IV.4”. Figure IV.6 represents the change of current density in terms of the voltage and the quantum efficiency of CIGS based solar cells respectively to several values of the relative permittivity of ZnO window layer

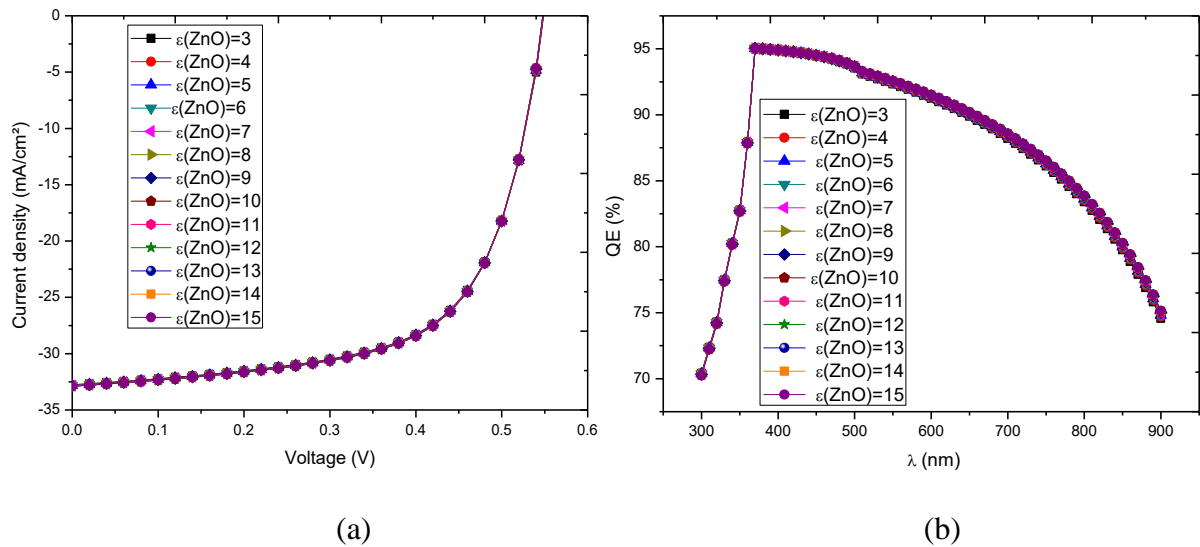
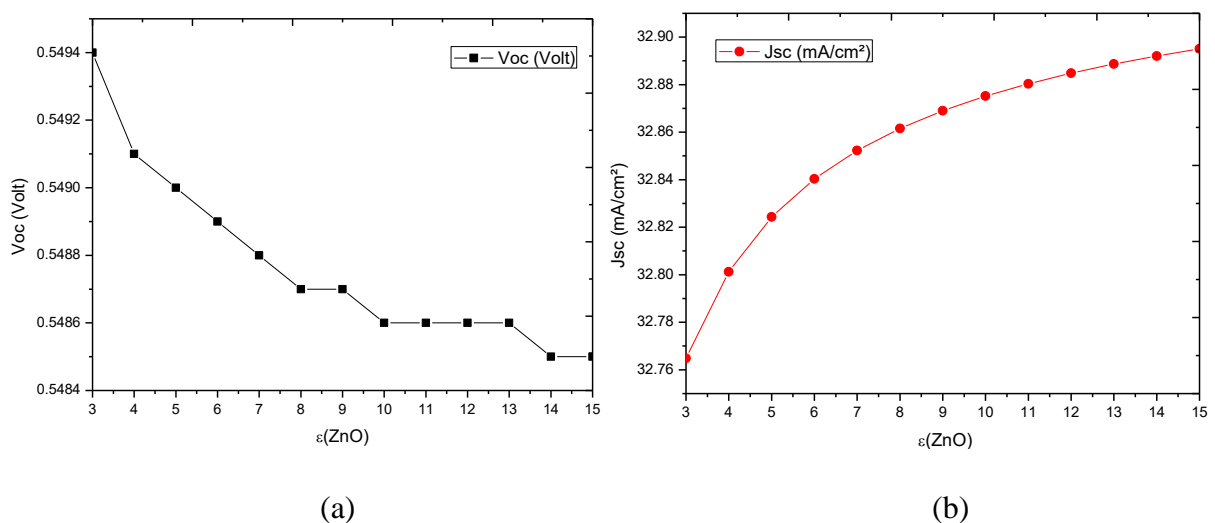


Figure IV.6: (a) The J-V characteristic for ZnO window layer where $\epsilon_{(\text{CdS})} = 15$ and $\epsilon_{(\text{CIGS})}$ layer is constant and equal to 13.6, (b) the quantum efficiency.

We notice that the current and the voltage is not affected when the value of the relative permittivity of the ZnO window layer increases. The increase in the relative permittivity is not affect in the quantum efficiency, so the number of the generated electrons-holes pairs, thus the current stay constant. The open circuit voltage is constant for the internal voltage is not affected by the increase in the relative permittivity.

Figure IV.7 show the effect of the relative permittivity of ZnO window layer in: the open circuit voltage, short circuit current density, the fill factor and the efficiency.respectively.



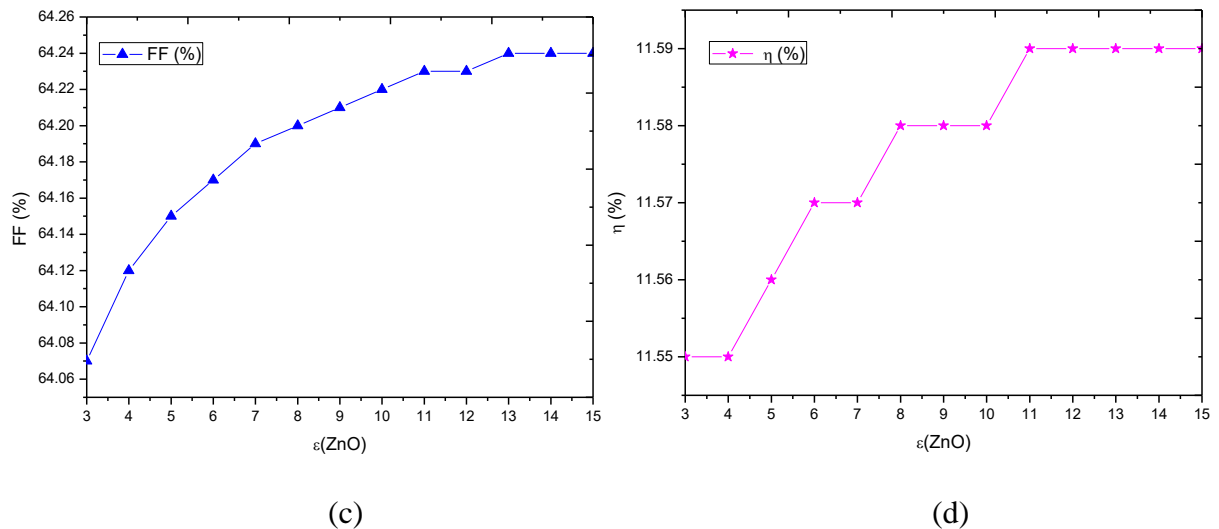


Figure IV.7: The effect of the relative permittivity of ZnO window layer in: (a) open circuit voltage, (b) short circuit current density, (c) the fill factor and (d) the efficiency.

We notice that the J-V characteristic is not affected for the changing in values of the relative permittivity of ZnO window layer.

We notice that the open circuit voltage in the first ($\epsilon = 3$) has a high value ($V_{oc} = 0.5494 \text{ V}$) and after decrease slowly to a minimum value ($\epsilon = 14$) and stay constant for. $\epsilon = 15$. The short circuit current, and the fill factor increase with the increase of the relative permittivity of the ZnO window layer. This lead to the outcome of these changes gives the effect on the solar cell's efficiency that increase slightly from 11.53 % to a greater value, which is 11.59 %.

IV.4.1.3 The influence of the relative permittivity of CIGS absorber layer

Figure IV.8 represents the change of current density in terms of the voltage and the quantum efficiency of CIGS based solar cells respectively to several values of the relative permittivity of CIGS absorber layer.

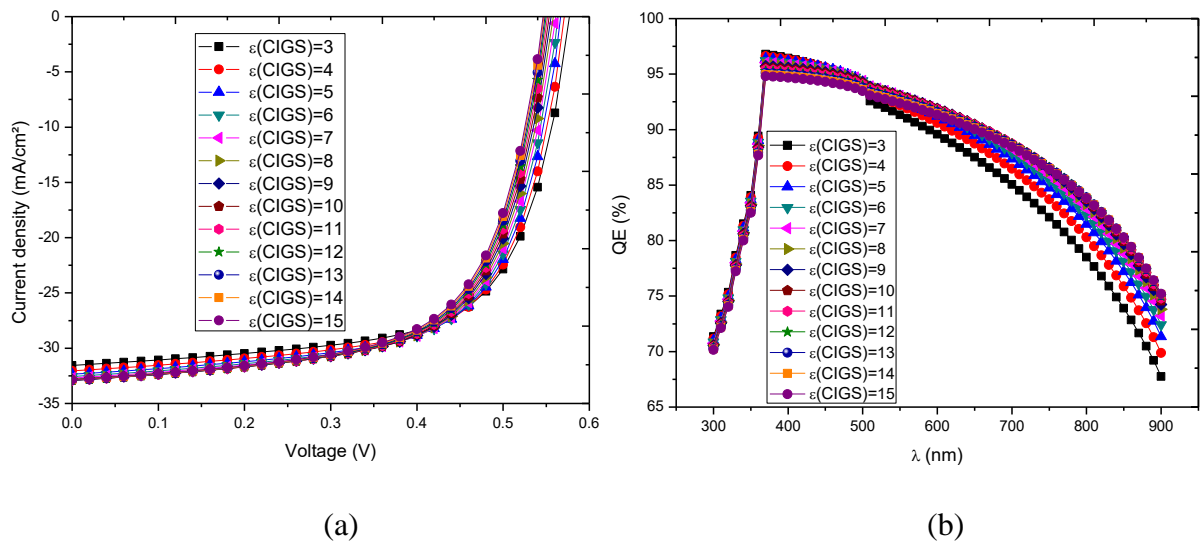
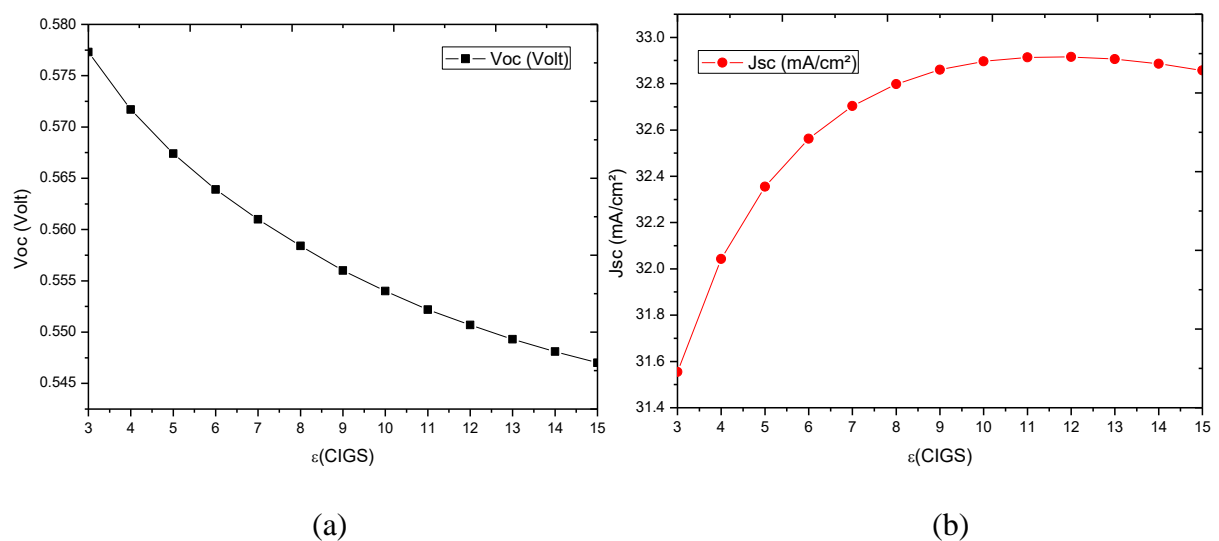


Figure IV.8: (a) The J - V characteristic for CIGS absorber layer where $\epsilon(\text{CdS})$ and $\epsilon(\text{ZnO})$ equal to 15, (b) the quantum efficiency.

We notice that the current increases when the value of the relative permittivity of the CIGS absorber layer increases. The increase in the relative permittivity increases the quantum efficiency, which gives an increase in the number of the generated electrons-holes pairs and thus increase the current. The open circuit voltage decrease for the internal voltage is affected by the increase in the relative permittivity.

Figure IV.9 show the effect of the relative permittivity of **CIGS** absorber layer in: the open circuit voltage, short circuit current density, the fill factor and the efficiency. respectively



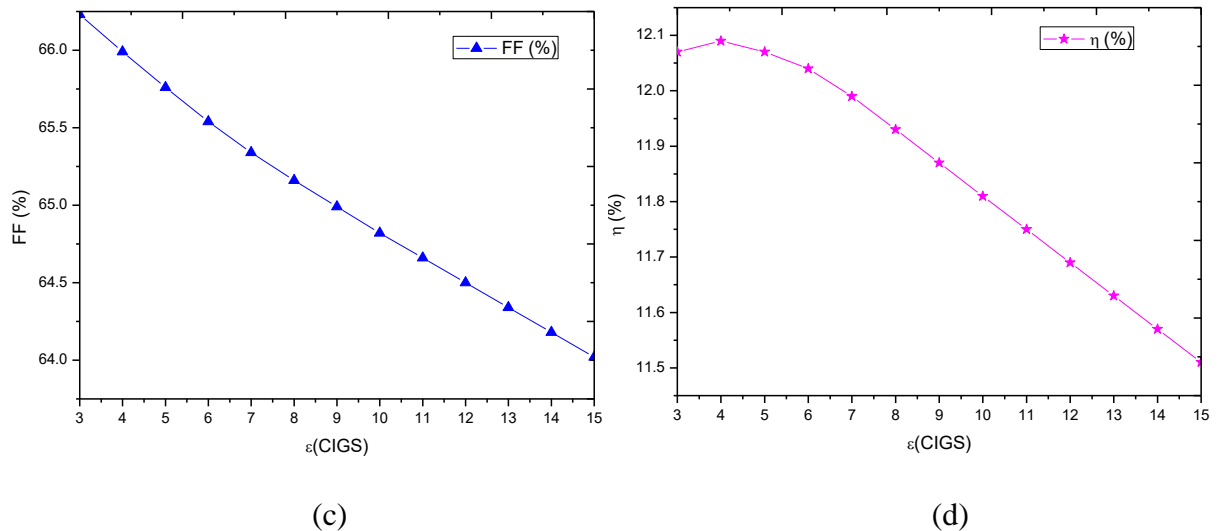


Figure IV.9: The effect of the relative permittivity of CIGS absorber layer in: (a) open circuit voltage, (b) short circuit current density, (c) the fill factor, (d) the efficiency.

We notice that the J-V characteristic improves for the big values of the relative permittivity of CIGS absorber layer.

We notice that the open circuit voltage and the fill factor decrease rapidly with the increase of the relative permittivity of CIGS effective layer. The short circuit current increases with the increase of the CIGS relative permittivity. This lead to the outcome of these changes gives the effect on the solar cell's efficiency where when ($\epsilon = 3; \eta = 12.07\%$) and for ($\epsilon = 4$), it increases to a big value ($\eta = 12.09\%$) and after decrease rapidly from 12.09 % to a lower value, which is 11.51 %.

General conclusion

In this work, we have studied the effect of the relative permittivity on CIGS based solar cells by a numerical simulation using SCAPS software. The CIGS device is based on CIGS as the effective layer and *CdS* as the other part of the p-n heterojunction. The purpose of this study is to prove that the permittivity can also affect the solar cells figures of merit.

The mainly extracted electrical parameters are the J-V characteristic, the quantum efficiency and the outputs of the cell: the open circuit voltage V_{oc} , the short circuit current density J_{sc} , the fill factor FF and the conversion efficiency η .

We have changed the permittivity of the three layers (*CdS*, *ZnO* and CIGS) from $\epsilon = 3$ to 15 we have found that:

- ✓ Whenever the permittivity for *CdS* layer increases, the efficiency increases. At $\epsilon = 15$; the efficiency improves to 11.58 %. We deduce that high permittivity materials is the preferred choice for the heterojunction partner for the absorber layer.
- ✓ When the permittivity of *ZnO* window layer is varied in the two cases ($\epsilon(\mathbf{CdS}) = 10$) and ($\epsilon(\mathbf{CdS}) = 15$) respectively, it is found that the efficiency does not vary much (from 11.19 % to 11.27 % and from 11.53 % to 11.59 %).
- ✓ For the CIGS absorber layer, it is found that the effective layer material that has $\epsilon = 4$ is the best choice for a good performance to form a CIGS based solar cells.

References

- [1] P. C. Choubey, A. Oudhia, and R. Dewangan. "A review: Solar cell current scenario and future trends", *Recent Research in Science and Technology*, 4.8, 2012.
- [2] A. Chirilă., S. Buecheler, F. Pianezzi, P. Bloesch, C. Gretener, A. R. Uhl, and R. Verma, "Highly efficient Cu (In, Ga) Se 2 solar cells grown on flexible polymer films", *Nature materials*, 10(11), 857, 2011.
- [3] T. Markvart, A. McEvoy, and L. Castaner, "Practical handbook of photovoltaics: fundamentals and applications", Elsevier, 2003.
- [4] I. Aguilera, J. Vidal, P. Wahnón, L. Reining and S. Botti, "First-principles study of the band structure and optical absorption of CuGaS₂", *Physical Review B*, 84(8), 085145, 2011.
- [5] N. Khoshsirat and N. A. M. Yunus, "Numerical simulation of CIGS thin film solar cells using SCAPS-1D", *Conference on Sustainable Utilization and Development in Engineering and Technology (CSUDET)*, pp: 63-67, IEEE, May, 2013.
- [6] A. Crovetto, M. K. Huss-Hansen and O. Hansen, "How the relative permittivity of solar cell materials influences solar cell performance", *Solar Energy*, 149, 145-150, 2017.
- [7] P. Hersch and K. Zweibel, "Basic photovoltaic principles and methods (No. SERI/SP-290-1448), Solar Energy Research Inst., Golden, CO (USA), pp: 9, 1982.
- [8] S. Sharma, K. K. Jain and A. Sharma, "Solar cells: in research and applications—a review", *Materials Sciences and Applications*, 6(12), 1145, 2015.
- [9] M. Sadok, « Détermination des Paramètres, Performances et Etude de la Dégradation des Modules Photovoltaïques en milieu saharien », these de doctorat, Université Aboubakr Belkaid – Tlemcen, 2011.
- [10] V. Foncrose, « Nanocristaux, films et cellules photovoltaïques de Cu₂ZnSn (SSe) 4 par impression d'encre », Doctoral dissertation, Université de Toulouse, Université Toulouse III-Paul Sabatier, 2015.
- [11] B. Abdeldjabar, "Simulation d'une cellule solaire photovoltaïque à base de Cu₂ZnSn(S, Se) 4", these de doctorat, Université de Ouargla, 06/06/2017.
- [12] M. Lasladj, « Simulation numérique des cellules solaires de troisième génération pour des applications spatiales », Doctoral dissertation, Université F.A de Sétif-1, 2015.

- [13] K. Ranabhat, L. Patrikeev, A. Antal'evna-Revina, K. Andrianov, V. Lapshinsky, and E. Sofronova, "An introduction to solar cell technology", *Journal of Applied Engineering Science*, Vol.14, No. 4, pp: 481-491, 2016.
- [14] P. Jayakumar, "Solar Energy Resource Assessment Handbook", p 117, September 2009.
- [15] I. Mallem, « Simulation des cellules solaires hétérojonction Si-SiGe par SILVACO » (Doctoral dissertation, Université Mohamed Khider-Biskra, 2014).
- [16] C. J. Chen, "Physics of solar energy", John Wiley & Sons, 2011.
- [17] A. Mcevoy, L. Castaner and T. Markvart, "Solar cells: materials, manufacture and operation", Academic Press, 2012.
- [18] M. Bertolli, "Solar Cell Materials", Course: Solid State II, In Department of Physics, University of Tennessee, 2008.
- [19] S. Kasap, and P. Capper, "Springer handbook of electronic and photonic materials", Springer, 2017.
- [20] A. M. Bagher, M. M. A. Vahid, and M. Mohsen, "Types of solar cells and application", *American Journal of optics and Photonics*, 3(5), 94-113, 2015.
- [21] M. Mostefaoui, H. Mazari, S. Khelifi, A. Bouraiou, and R. Dabou, "Simulation of high efficiency CIGS solar cells with SCAPS-1D software", *Energy Procedia*, 74, 736-744, 2015.
- [22] A. Luque, and S. Hegedus, "Photovoltaic science and engineering", Chichester: John Wiley & Sons Ltd, 2003.
- [23] J. Löckinger, S. Nishiwaki, T. P. Weiss, B. Bissig, Y. E. Romanyuk, S. Buecheler and A. N. Tiwari, "TiO₂ as intermediate buffer layer in Cu (In, Ga) Se₂ solar cells", *Solar Energy Materials and Solar Cells*, 174, 397-404, 2018.
- [24] M. Nakamura, N. Yoneyama, K. Horiguchi, Y. Iwata, K. Yamaguchi, H. Sugimoto, and 40th Photovoltaic Specialist Conference (PVSC) (pp. 0107-0110), IEEE, June 2014.
- [25] J. E. Jaffe, A. Zunger, *J. Phys*, "Chem.Sol", 64, 1547, 2003.
- [26] C. Roger, « Développement de cellules photovoltaïques à base de CIGS sur substrats métalliques », Doctoral dissertation, Grenoble, 2013.

- [27] A. Duchatelet, « Synthèse de couches minces de Cu (In, Ga) Se₂ pour cellules solaires par électrodépôt d'oxydes mixtes de cuivre-indium-gallium », Doctoral dissertation, Lille 1, 2012
- [28] D. K. Suri, K. C. Nagpal, and G. K. Chadha, "X-ray study of CuGa_xIn_{1-x}Se₂ solid solutions", *Journal of Applied Crystallography*, 22(6), 578-583, 1989.
- [29] K. Zeaiter, Y. Llinares, and C. Llinares, "Structural and photoluminescence study of the quaternary alloys system CuIn (S_xSe_{1-x})₂", *Solar energy materials and solar cells*, 61(3), 313-329, 2000.
- [30] W. N. Shafarman, S. Siebentritt, and L. Stolt, "Cu (InGa) Se₂ Solar Cells », *Handbook of photovoltaic science and engineering*, 546-599, 2010.
- [31] J. S. Park, Z. Dong, S. Kim, and J. H. Perepezko, "CuInSe₂ phase formation during Cu₂Se/In₂Se₃ interdiffusion reaction", *Journal of Applied Physics*, 87(8), 3683-3690, 2000.
- [32] K. J. Bachmann, H. Goslowky, and S. Fiechter, "The phase relations in the system Cu, In, Se", *Journal of crystal growth*, 89(2-3), 160-164, 1988.
- [33] D. Rudmann, "Effects of sodium on growth and properties of Cu (In, Ga) Se₂ thin films and solar cells", Doctoral dissertation, ETH Zurich, 2004.
- [34] T. P. Hsieh, C. C. Chuang, C. S. Wu, J. C. Chang, J. W. Guo, and W. C. Chen, "Effects of residual copper selenide on CuInGaSe₂ solar cells", *Solid-State Electronics*, 56(1), 175-178, 2011.
- [35] U. C. Boehnke and G. Kühn, "Phase relations in the ternary system Cu-In-Se", *Journal of materials science*, 22(5), 1635-1641, 1987.
- [36] S. B. Zhang, S. H. Wei, A. Zunger, and H. Katayama-Yoshida, "Defect physics of the CuInSe₂ chalcopyrite semiconductor", *Physical Review B*, 57(16), 9642, 1998.
- [37] P. Panse, "Copper gallium diselenide solar cells: Processing, characterization and simulation studies", 2003.
- [38] K. Siemer, J. Klaer, I. Luck, J. Bruns, R. Klenk and D. Bräunig, "Efficient CuInS₂ solar cells from a rapid thermal process (RTP)", *Solar Energy Materials and Solar Cells*, 67(1-4), 159-166, 2001.
- [39] M. Saad, H. Riazi, E. Bucher, and M. C. Lux-Steiner, "CuGaSe₂ solar cells with 9.7% power conversion efficiency", *Applied Physics A*, 62(2), 181-185, 1996.

- [40] I. Repins, M. A. Contreras, B. Egaas, C. DeHart, J. Scharf, C. L Perkins, and R. Noufi, “19.9%-efficient ZnO/CdS/CuInGaSe₂ solar cell with 81.2% fill factor”, *Progress in Photovoltaics: Research and applications*, 16(3), 235-239, 2008.
- [41] P. R. Jackson, U. Würz, J. Rau, T. Kurth, G. Schlotzer, Bilger, and J. H. Werner, “high quality baseline for high efficiency, Cu(In_{1-x}, Ga_x)Se₂ solar cells”, *Progress in Photovoltaics :Research and Applications*, Vol. 15, No. 6, pp: 507-519, 2007.
- [42] P. Jackson, D. Hariskos, E. Lotter, S. Paetel, R. Würz, R. Menner and M. Powalla, “New world record efficiency for Cu (In, Ga) Se₂ thin-film solar cells beyond 20%”, *Progress in Photovoltaics: Research and Applications*, 19(7), 894-897, 2011.
- [43] B. Equer, « *Energie solaire photovoltaïque* », Vol.1, Ellipses, 1993.
- [44] A. Luque, “*Practical Handbook of Photovoltaics*”, (Second Edition), 2012.
- [45] J.I. Pankove, “*Optical Process in Semiconductors*”, Dover, New York, 1971.
- [46] Y.P. Varshni, “*Physica*”, 34,149,1967.
- [47] J. Ramanujam, and U. P. Singh, “Copper indium gallium selenide based solar cells—a review”, *Energy & Environmental Science*, 10(6), 1306-1319, 2017.
- [48] A. Shah, P. Torres, R. Tscharnner, N. Wyrsh and H. Keppner, “Photovoltaic technology: the case for thin-film solar cells”, *science*, 285(5428), 692-698, 1999.
- [49] M. Khan and M. Islam, “Deposition and characterization of molybdenum thin films using dc-plasma magnetron sputtering”, *Semiconductors*, 47(12), 1610-1615, 2013.
- [50] M. Doriani, H. D. Jahromi and M. H. Sheikhi, “A Highly Efficient Thin Film CuInGaSe₂ Solar Cell”, *Journal of Solar Energy Engineering*, 137(6), 064501, 2015.
- [51] A. Bouraiou, « *Elaboration et caractérisation des couches minces CuInSe₂ par électrodéposition* », 2009.
- [52] https://users.elis.ugent.be/SCAPS_introduction.pdf.
- [53] A. Niemegeers, M. Burgelman, K. Decock, J. Verschraegen and S. Degraeve, “*SCAPS manual*”, University of Gent, 2014.
- [54] <https://www.utoledo.edu/radther/pdf>.

Abstract

SCAPS software is used to study the effect of the relative permittivity on CIGS based solar cells. It is found that whenever the *CdS* layer permittivity increases, the efficiency increases. It is deduced that high permittivity materials are preferred as the heterojunction partner of the absorber layer. It is also found that the permittivity of the *ZnO* window layer does not affect the solar cell performance. On the other hand, for CIGS layer, $\epsilon = 4$ was to be the best choice.

Key words: Permittivity, CIGS solar cells, numerical simulation, J-V characteristic, SCAPS software.

ملخص

يستخدم برنامج SCAPS لدراسة تأثير السماحية النسبية على الخلايا الشمسية القائمة على CIGS. لقد وجد أنه كلما زادت سماحية طبقة CdS ، تزداد الكفاءة. يستنتج أن المواد ذات السماحية العالية مفضلة كشرط متغاير لطبقة الامتصاص. وجد أيضًا أن سماحية طبقة نافذة ZnO لا تؤثر على أداء الخلية الشمسية. من ناحية أخرى بالنسبة لطبقة CIGS ، كان $\epsilon = 4$ هو الخيار الأفضل.

الكلمات المفتاحية : السماحية، الخلايا الشمسية من CIGS، محاكاة رقمية، الخاصية J-V، برنامج SCAPS.

Abstract

SCAPS software is used to study the effect of the relative permittivity on CIGS based solar cells. It is found that whenever the *CdS* layer permittivity increases, the efficiency increases. It is deduced that high permittivity materials are preferred as the heterojunction partner of the absorber layer. It is also found that the permittivity of the *ZnO* window layer does not affect the solar cell performance. On the other hand, for CIGS layer, $\epsilon = 4$ was to be the best choice.

Key words: Permittivity, CIGS solar cells, numerical simulation, J-V characteristic, SCAPS software.

ملخص

يستخدم برنامج SCAPS لدراسة تأثير السماحية النسبية على الخلايا الشمسية القائمة على CIGS. لقد وجد أنه كلما زادت سماحية طبقة CdS ، تزداد الكفاءة. يستنتج أن المواد ذات السماحية العالية مفضلة كشريك متغاير لطبقة الامتصاص. وجد أيضًا أن سماحية طبقة نافذة ZnO لا تؤثر على أداء الخلية الشمسية. من ناحية أخرى بالنسبة لطبقة CIGS ، كان $\epsilon = 4$ هو الخيار الأفضل.

